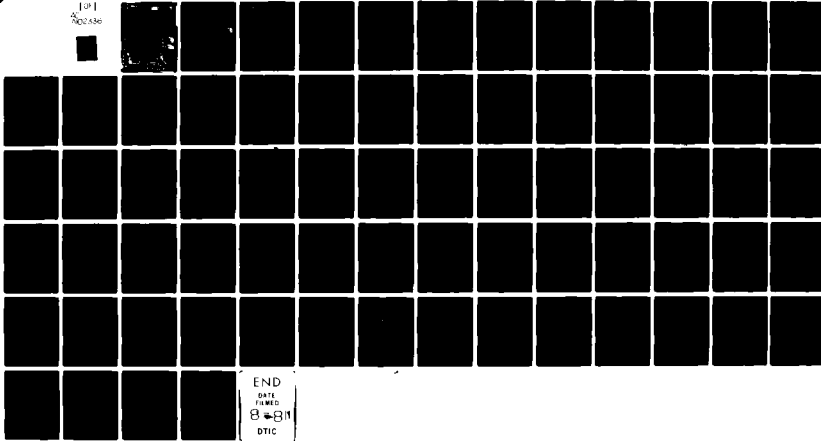


AD-A102 336

SCIENCE APPLICATIONS INC CANOGA PARK CA COMBUSTION D--ETC F/G 21/5  
COMBUSTION IN HIGH SPEED AIR FLOWS.(U)  
JUN 81 W N BRAGG, J C CHIEN, G C COOPER F49620-80-C-0082  
SAI-81-030-CP AFOSR-TR-81-0594 NL

UNCLASSIFIED

(u)  
2025 Dec 06



END

DATE

FILED

8-81

DTIC

AD A102336

Approved for public release  
Government of Canada

CRIS  
C-3  
AUG 3 1984  
D

SCIENCE APPLICATIONS, INC.  
A SUBSIDIARY OF SCIENTIFIC-COMPUTER SYSTEMS, INC.

81-3889-161

3

COMBUSTION IN HIGH SPEED AIR FLOWS

Interim Technical Report  
1 April 1980 - 31 March 1981

by

W. N. Bragg  
J. C. Chien  
G. C. Cooper  
R. B. Edelman  
P. T. Harsha

Science Applications, Inc.  
Combustion Science and Advanced Technology Department  
21133 Victory Boulevard  
Canoga Park, California 91303

DTIC  
SELECTED  
AUG 3 1981  
S D C

prepared for

Air Force Office of Scientific Research  
Bolling Air Force Base  
Washington, D. C. 20332

June 1981

DISTRIBUTION STATEMENT A  
Approved for public release;  
Distribution Unlimited

UNCLASSIFIED

~~SECURITY CLASSIFICATION OF THIS PAGE (When Data Entered)~~

REPORT DOCUMENTATION PAGE		READ INSTRUCTIONS BEFORE COMPLETING FORM	
<b>AFOSR-TR--81-0594</b>		2. GOVT ACCESSION NO.	
4. TITLE (and Subtitle)		3. RECIPIENT'S CATALOG NUMBER	
Combustion in High Speed Air Flows,		9 Interim Rept. Apr 1980 - Apr 1981	
7. AUTHOR(s) W. N. Bragg, J. C. Chien, G. C. Cooper, R. B. Edelman and P. T. Harsha		5. TYPE OF REPORT & PERIOD COVERED PERIODIC REPORT NUMBER SAI-81-030-CP	
9. PERFORMING ORGANIZATION NAME AND ADDRESS Science Applications, Inc. 21133 Victory Blvd. Canoga Park, CA 91303		6. CONTRACT OR GRANT NUMBER(s) F49620-80-C-0082	
11. CONTROLLING OFFICE NAME AND ADDRESS Air Force Office of Scientific Research Bldg 410 Bolling Air Force Base, D.C. 20332		10. PROGRAM ELEMENT, PROJECT, TASK AREA & WORK UNIT NUMBERS 61102F 12348/A21	
14. MONITORING AGENCY NAME & ADDRESS (if different from Controlling Office)		12. REPORT DATE June 1981	
16. DISTRIBUTION STATEMENT (of this Report)		13. NUMBER OF PAGES 72	
Approved for Public Release, distribution unlimited		15. SECURITY CLASS. (of this report) Unclassified	
17. DISTRIBUTION STATEMENT (of the abstract entered in Block 20, if different from Report)		15a. DECLASSIFICATION/DOWNGRADING SCHEDULE	
18. SUPPLEMENTARY NOTES			
19. KEY WORDS (Continue on reverse side if necessary and identify by block number)			
Sudden Expansion (Dump) Burner Integral Rocket/Ramjet Engine Recirculating Reacting High Speed Flow Flowfield Modeling Boron Slurry Fuels		Ducted Rocket Combustor	
20. ABSTRACT (Continue on reverse side if necessary and identify by block number)			
Progress in research into fundamental mechanisms of combustion in high speed air flows is described. Three major areas are covered: the application of a modular combustor model for the liquid fueled sudden expansion combustor configuration to the analysis of flame stability and the interpretation of combustor test data; the extension of the modular model to the analysis of boron slurry fueled ramjet combustors; and, the development of analytical models of the ducted rocket combustor. The modular approach is demonstrated to be a useful tool for the analysis and interpretation of sudden-expansion combustor			

DD FORM 1473 EDITION OF 1 NOV 65 IS OBSOLETE  
JAN 73

**UNCLASSIFIED**  
SECURITY CLASSIFICATION OF THIS PAGE (When Data Entered)

~~UNCLASSIFIED~~

*Unclassified*

SECURITY CLASSIFICATION OF THIS PAGE(When Data Entered)

20. → flame stabilization phenomena and to be of considerable utility in the analysis of combustor test data. Models for the combustion of boron particles are reviewed and put into a form suitable for incorporation in a modular model of a boron slurry fueled combustor. Particle tracking methods suitable for use in the context of a modular model formulation have been defined and developed for the required application. The approach required to provide an analytical model of the three-dimensional recirculating flow in a ducted rocket combustor has been defined and the development of an aerodynamic model has been initiated.

Accession For	
NTIS GRA&I	<input type="checkbox"/>
DTIC TAB	<input type="checkbox"/>
Unannounced	<input type="checkbox"/>
Justification	
By	
Distribution/	
Availability Codes	
Avail and/or	
Dist	Special
A	
?	

*Unclassified*

SECURITY CLASSIFICATION OF THIS PAGE(When Data Entered)

## TABLE OF CONTENTS

<u>Section</u>	<u>Title</u>	<u>Page</u>
1	Introduction . . . . .	1
2	The Application of Modular Modeling to Ramjet Performance Investigations . . . . .	5
3	Modifications to Modular Model for Boron Slurry Fuel Combustion . . . . .	19
	3.1 Boron Ignition and Combustion Models . . . . .	21
	3.2 Boron Particle Combustion Subroutines for the Modular Model . . . . .	23
	3.2.1 King's Model . . . . .	35
	3.2.2 Edelman's Model . . . . .	40
	3.3 Particle Tracking for Slurry Fuel Combustion Analyses . . . . .	49
	3.4 Summary . . . . .	57
4	Formulation of a Mathematical Model of a Ducted Rocket Combustor . . . . .	59
5	Overall Summary and Future Work . . . . .	64
6	References . . . . .	66

AIR FORCE OFFICE OF SCIENTIFIC RESEARCH (AFSC)  
NOTICE OF TRANSMITTAL TO DDC  
This technical report has been reviewed and is  
approved for public release IAW AFR 190-12 (7b).  
Distribution is unlimited.  
A. D. BLOSE  
Technical Information Officer

## ABSTRACT

Progress in research into fundamental mechanisms of combustion in high speed air flows is described. Three major areas are covered: the application of a modular combustor model for the liquid fueled sudden expansion combustor configuration to the analysis of flame stability and the interpretation of combustor test data; the extension of the modular model to the analysis of boron slurry fueled ramjet combustors; and the development of analytical models of the ducted rocket combustor. The modular approach is demonstrated to be a useful tool for the analysis and interpretation of sudden-expansion combustor flame stabilization phenomena and to be of considerable utility in the analysis of combustor test data. Models for the combustion of boron particles are reviewed and put into a form suitable for incorporation in a modular model of a boron slurry fueled combustor. Particle tracking methods suitable for use in the context of a modular model formulation have been defined and developed for the required application. The approach required to provide an analytical model of the three-dimensional recirculating flow in a ducted rocket combustor has been defined and the development of an aerodynamic model has been initiated.

## 1. INTRODUCTION

Design trends for current and future airbreathing propulsion systems are trending toward lower weight and smaller volume designs. These requirements, and increased demands for higher performance from airbreathing propulsion systems in general and ramjet devices in particular, have resulted in the need to upgrade existing technologies to meet the emergence of more stringent design requirements. Achieving reduced volume and weight requires the use of shorter combustors and high energy, high density fuels. Systems constraints have dictated the use of sudden-expansion (dump) combustors capable of operating effectively at high combustion intensities over wide ranges of conditions. Problems of flame stabilization, flame propagation and spray combustion have been encountered. To aid in the development of solutions to these problems, analytical combustor models are a requirement: the ability to compute in some detail combustion chamber flowfields is necessary in order to understand the phenomena that occur in existing combustors and to predict the performance of new combustor concepts. The insight gained through the use of analytical combustor models can be of substantial value in the planning of a combustor test program and in the interpretation of combustor and combustor component test data.

In response to the needs just outlined, a detailed model of the sudden-expansion liquid fueled ramjet combustor has been developed, as part of earlier AFOSR-sponsored work (Ref. 1). This model makes use of the modular concept, in which the combustor flowfield, represented schematically in Fig. 1, is broken down into three major components: a directed flow, which is treated as parabolic, a recirculation zone, assumed to be represented by well-stirred reactor(s), and a turbulent shear layer along the dividing streamline which separates the other two regions. The shear layer serves as the coupling region between the other two model components; fluxes of species and energy across this shear layer form the boundary conditions on the two computational regions. Finite-rate chemistry, based on the quasiglobal model (Ref. 2) is included in the formulations for both the directed flow and well-stirred reactor regions, although for the modular model calculations described in this paper, the recirculation region well-stirred reactor formulation has been restricted to a global finite-rate chemistry model. The directed flow is

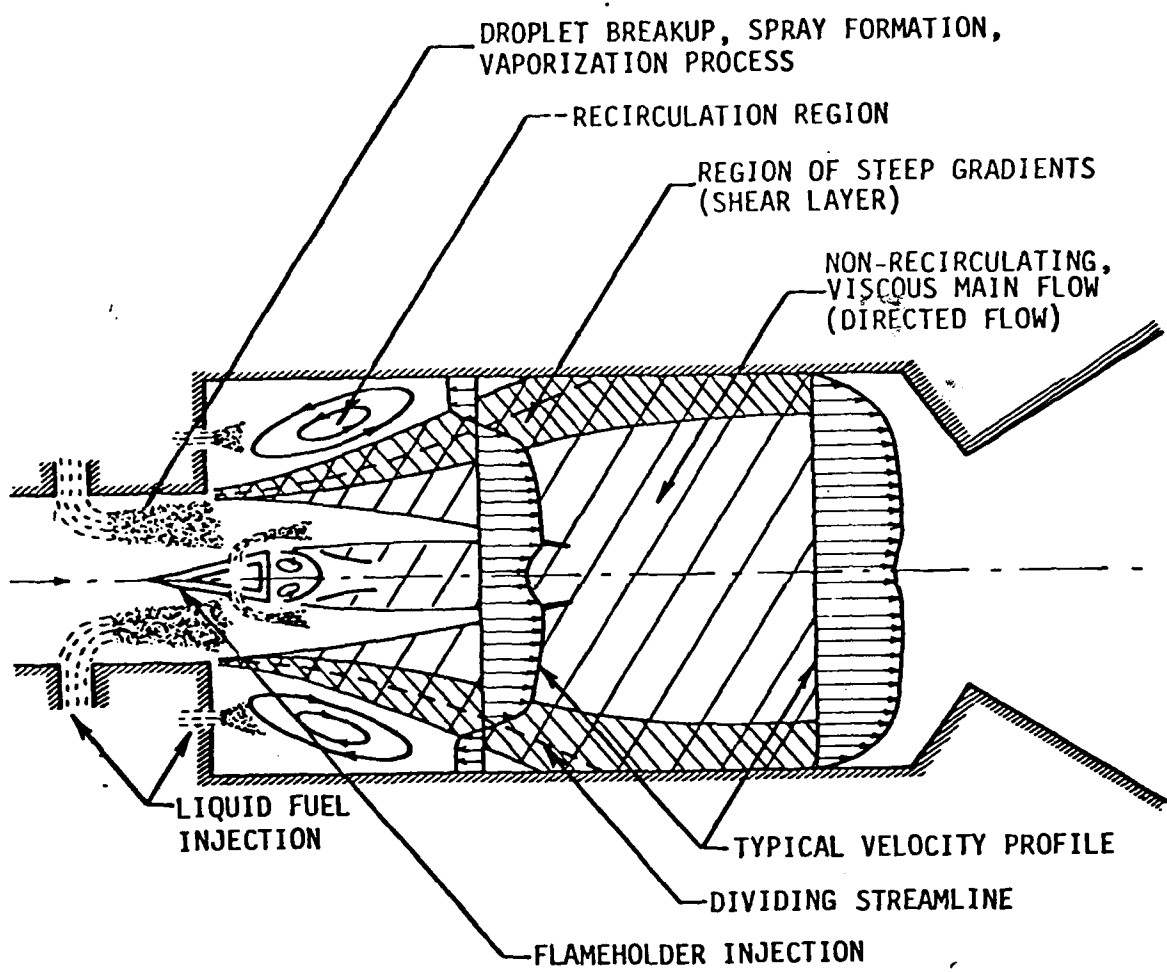


Figure 1. Schematic of Sudden-Expansion (Dump) Burner.

assumed to be fully turbulent, with the turbulent viscosity defined by a two-equation turbulence model (Ref. 3). A key feature of this approach is the provision for the shear layer coupling region in the model. Through the use of this element of the model, the division of the mass flux between the directed flow and the recirculation region is computed iteratively rather than specified empirically. Furthermore, the directed flow region is computed in detail as a two-dimensional parabolic flowfield, rather than through a one-dimensional approximation, allowing the use of detailed computations of the mixing and chemical reactions in this region of the combustor.

A variety of results obtained in the process of validating the modular model approach for the prediction of ramjet combustor performance and flow-field characteristics have been described in Refs. 1 and 4. During the current program, attention has been focused on further development of certain of the fundamental elements of the model, with particular emphasis on the stirred-reactor representation of flame-stabilizing recirculation regions. Other aspects of the current work include the development of boron combustion models and the definition of modeling approaches for ducted rocket combustor configurations.

Both gas generator ramjets (ducted rockets) and slurry-fueled ramjets are examples of propulsion devices which involve the turbulent mixing and combustion of multi-phase flows. In both of these applications boron-loaded fuels are of considerable interest because of their high energy content, and for both of these systems it is desirable to develop models which can aid in obtaining a fundamental understanding of the phenomena involved in two-phase mixing and combustion and which can be used to parametrically assess combustor performance. This need is being addressed in two of the tasks that are part of the current program. For boron slurry-fueled ramjets, the approach being taken involves a direct extension of the modular modeling approach developed for liquid-fueled ramjets and described in Refs. 1 and 4, while the application of modular modeling to the more complex geometry associated with the ducted rocket configuration is also being investigated. In the latter work, the approach being followed involves the development of a three-dimensional elliptic Navier-Stokes solution technique to be used to delineate the flowfield regions that are to be described by separate elements of the modular approach. This solution procedure is being developed to

obtain the cold-flow aerodynamics of the combustor configuration; the detailed modeling of this configuration incorporating the effects of multiphase flow and chemical heat release is to be carried out using the modular approach.

The three subsequent sections of this report reflect the three main areas of investigation outlined above. Thus, in Section 2, further examination of the use of the modular model of a liquid-fueled sudden expansion combustor is described, with emphasis on the prediction of flame stabilization phenomena. A detailed model of the combustion dynamics inherent in a boron slurry-fueled ramjet combustor requires the development of models for the combustion of boron particles and of techniques for treating the details of the combustion of boron particle clouds, and progress in this area is discussed in Section 3. Then, in Section 4, the technique being utilized to develop a gas-generator fueled ramjet (ducted rocket) aerodynamic model is described, and the overall progress made during this program is summarized in Section 5. In each of these areas close coordination has been maintained with government laboratory experimental work, including liquid-fueled ramjet and ducted rocket investigations underway at the Aeropropulsion Laboratory of the Air Force Wright Aeronautical Laboratory (AFWAL) and boron-slurry ramjet and ducted rocket work underway at the Naval Weapons Center (NWC) under joint AFOSR/NWC sponsorship.

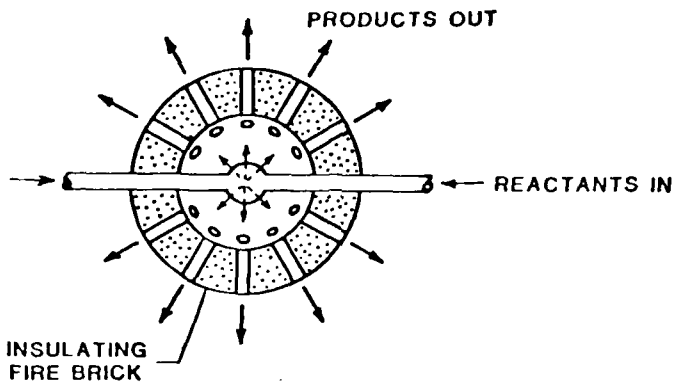
## 2. THE APPLICATION OF MODULAR MODELING TO RAMJET PERFORMANCE INVESTIGATIONS\*

The well-stirred reactor, shown schematically in Fig. 2a, is a laboratory device in which very high mixing rates are achieved. In general, laboratory stirred reactors are designed to ensure that the mixture within the reactor is spatially uniform, so that unreacted feed material is continuously and uniformly mixed with combustion products, reacting for a time defined by the average residence time of the reactor before exiting. For the limit of perfect stirring, this average residence time is given simply by the ratio of the stirred reactor volume to the feed mass flux,  $V/\dot{m}$ ; the product mass flux is of course equal to the feed mass flux. In this limit the governing equations for the stirred reactor state reduce to algebraic relations (Ref. 4), which allows the use of rapid and efficient solution procedures, incorporating either global finite-rate kinetics or the more detailed quasiglobal kinetics formulation.

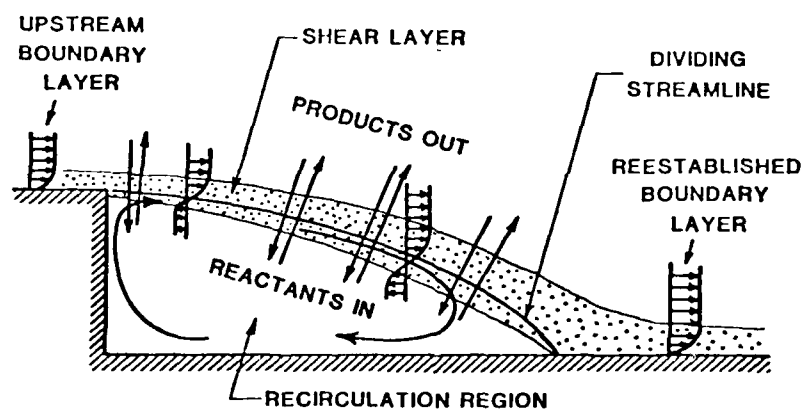
In the lower half of Fig. 2, a typical recirculation region in a sudden-expansion combustor is sketched. Because of the high turbulence intensity and large mixing rates generated in the flow reversal within the recirculation the limiting behavior of this region can be thought of as well-mixed; that is, the state of the recirculation region is defined by the chemical kinetics of the reactions occurring and not by the mixing rate. In this sense the volume within the recirculation region sketched in Fig. 2b is similar to the volume within the laboratory stirred reactor of Fig. 2a, and the same solution technique can be used to obtain the thermochemical state. A comparison of Figs. 2a and 2b also shows the major difference between the recirculation region and the laboratory stirred reactor. In the laboratory stirred reactor discrete reactant and product streams can be identified, but in the well-stirred reactor model of a sudden-expansion recirculation zone, separate reactant and product streams cannot be defined. Instead, reactants enter the recirculation region and products leave the recirculation region by turbulent diffusion through the shear layer, integrated over the surface area of the dividing streamline, and the product stream is defined similarly. These fluxes are of course equal and opposite.

---

\* The material incorporated in this section is taken from "Interpretation of Ramjet Combustor Test Data," by P. T. Harsha and R. B. Edelman, AIAA Paper 81-1433, to be presented at the AIAA/SAE/ASME 17th Joint Propulsion Conference, July 27-29, 1981.



(a) Schematic design of spherical well-stirred reactor.



(b) Schematic of sudden-expansion recirculation region flowfield.

FIGURE 2. Comparison of well-stirred reactor with recirculation region flowfield.

The fact that in the well-stirred reactor model of a sudden-expansion recirculation region the feed rates are defined by the fluxes of reactants and products through the shear layer region is the reason that this region has been identified as a key element of the modular model described in Refs. 1-3 and 6. Nevertheless, this shear layer is modeled fairly crudely as a region of linear gradients: that is, the gradient in a quantity  $\phi$  at the dividing streamline is approximated by

$$\left. \frac{\partial \phi}{\partial r} \right|_W = \frac{\phi_P - \phi_R}{\ell} \quad (1)$$

where the subscripts P, R, and W refer to conditions in the directed flow immediately outside of the recirculation zone, in the recirculation zone itself, and along the dividing streamline, respectively. Moreover, the width of the shear layer is assumed to be given by the linear expression

$$\ell = ax + b \quad (2)$$

in which a and b are constants to be defined through comparison of model predictions with experimental data.

As is described in more detail in Refs. 1, 4-6, the overall flowfield computation using the modular model proceeds as follows: a dividing streamline shape is assumed, and the shear layer width expression and shear stress distribution along the dividing streamline are specified, the latter through use of a specified "skin friction" coefficient. An initial state for the stirred reactor is assumed, which defines an initial guess for the species distribution and temperature within the recirculation zone. With these available as boundary conditions, a finite-difference computation of the mixing region external to the recirculation is carried out to the end of the recirculation region. This calculation defines the species mass fraction and temperature gradients along the dividing streamline, and these values are used as outlined above to obtain the stirred reactor feed rates. A new stirred reactor computation is carried out using these feed rates, resulting in a new specification of the species mass fractions and temperature within the recirculation region, and the parabolic mixing computation is repeated. This procedure

is continued until changes in the stirred reactor composition and temperature from computation to computation become small, typically 0.1%, at which point the coupling iteration has converged. The parabolic calculation is then carried out to the end of the combustion chamber, completing the solution.

The entrainment rate into the recirculation region is an important parameter in the overall combustor flowfield computation, and as the previous paragraph indicates, this parameter is not specified, but is calculated as a part of the modular model solution procedure. Thus it is of considerable interest to compare the entrainment rate computed by the model with experimental data. A variety of data for recirculation region entrainment rates was reviewed by Curran (Ref. 7) and the range of the observed correlations is shown in Fig. 3: these correlations are for both cold flow and hot flow. Also shown in Fig. 3 are the entrainment mass flux ratios predicted using the modular model in several different calculations, involving different area ratios and cold flow as well as reacting flow. Other results from many of these computations are described in Ref. 4. The range of correlations shown did not include data from the investigations for which the calculations shown in Fig. 3 were made; nevertheless, the predictions show reasonably good agreement with the observed correlations. Of particular significance is the fact that the predicted reduction of the entrainment rate with combustion compared to cold flow at the same area ratio is in agreement with the observations reported by Curran. This represents an important result, both from the standpoint of validation of the modular model approach, even though a relatively crude shear layer model has been used, and because it suggests a more systematic study that can be pursued using the analytical model to examine a wider range of operating conditions than those on which the correlations were originally based.

One of the most important determinants of liquid fueled ramjet performance is the fuel distribution at the combustor entrance. For the sudden-expansion liquid fueled ramjet, the interaction between inlet fuel distribution and recirculation zone state is a further important consideration. A variety of observations have shown that for wall injection of the fuel, the recirculation zone equivalence ratio is generally more fuel-rich than the overall (global) equivalence ratio. This is demonstrated by the data of Schmotolocha and Economos (Ref. 8), which was obtained for three different inlet conditions

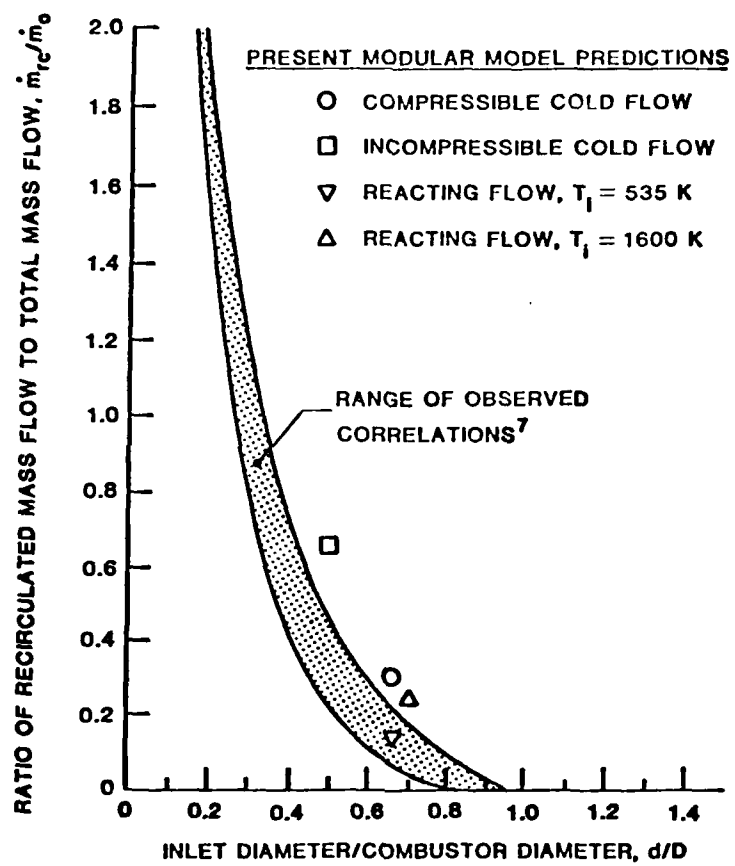


FIGURE 3. Comparison of measured and predicted entrainment rates.

and at two different locations of the fuel injection orifices upstream of the dump plane. Indeed, the measurements described in Ref. 8 indicate that for overall equivalence ratios greater than 0.2, the equivalence ratio in the recirculation region is always greater than unity. These data are shown in Fig. 4, in which the results of a modular model computation at one overall equivalence ratio are also shown. As was the case for the entrainment rate predictions, the agreement between the experimental results and the computation is reasonably good.

In the experiments described in Ref. 8 plain orifice fuel injection was used. For plain orifices, fuel penetration characteristics are reasonably well documented, and an empirical penetration correlation was used to establish initial conditions for the computations used to obtain the result shown in Fig. 4. However, plain orifices are not widely used in ramjet design because of their poor turndown characteristics which result in the need for several sets of orifices to obtain a wide ramjet operating range. The most commonly used fuel injector in liquid fuel ramjet applications is the poppet injector, which has a much broader turndown range than does a plain orifice. However, penetration characteristics from poppet injectors under ramjet operating conditions are not well documented. Indeed, there exists one investigation of poppet (and other nozzle) penetration characteristics under ramjet operating conditions in which it was observed that the penetration from poppets is essentially nil, Ref. 9. While other results indicate that penetration characteristics similar to orifice injection can be obtained using poppets, Ref. 10, it remains clear that the penetration characteristics of poppets are not as well known as for plain orifices.

At one operating condition, which involves a relatively high inlet temperature, poor ramjet combustor performance was observed in a recent development program: at this one condition performance was considerably poorer than at other test conditions. Review of the available results suggested that fuel distribution effects were a possible cause, and in particular that at the operating condition in question the fuel penetration from the wall-mounted fuel injectors may have been negligible. To investigate this possibility, and to study the effects of fuel distribution on combustor performance, a series of parametric modular model computations was carried out.

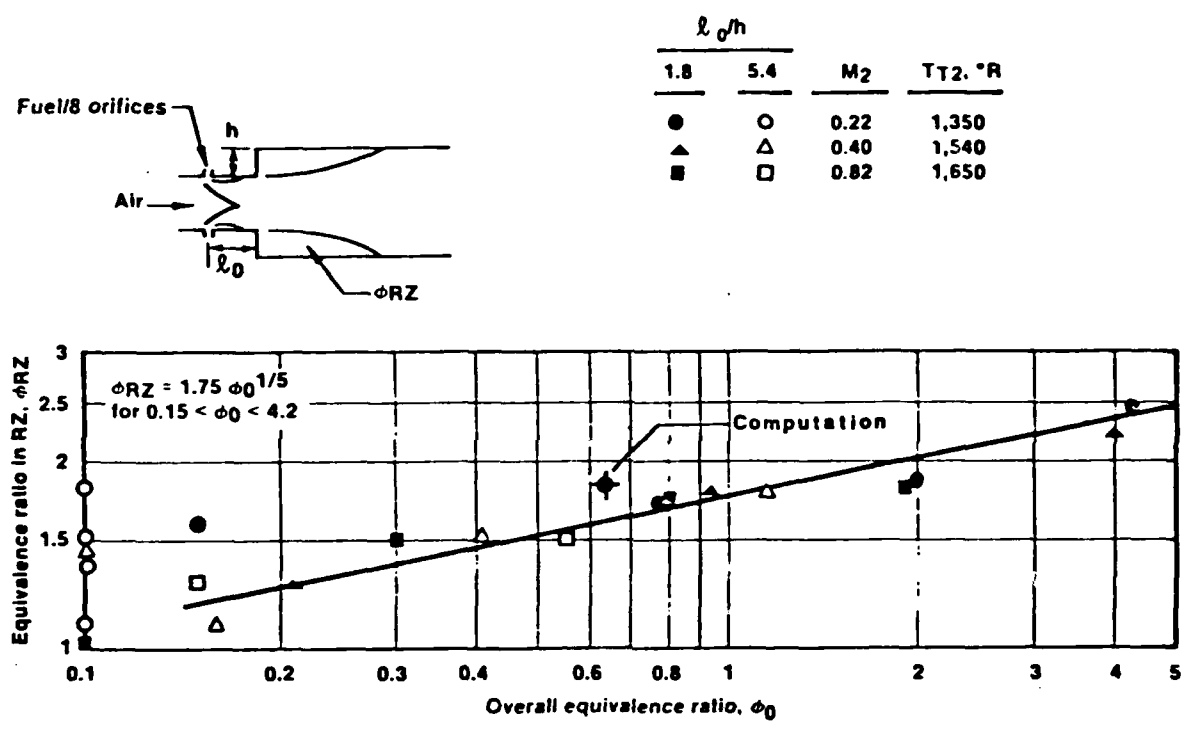


Figure 4. Fuel Concentration in Recirculation Zone

In the modular approach, fuel injection is modeled using an empirical correlation for penetration and breakup time correlation. The latter correlation defines the downstream position at which the penetration is computed; from this point the fuel spray is assumed to vaporize at a rate given by a bulk spray vaporization correlation. After injection, the fuel is assumed to reside in an annular region at the position specified by the penetration correlation, and spreading of this annulus is computed using a turbulent mixing model. For the conditions of interest in the parametric study, vaporization occurs rapidly, so that the parameter to be varied was the fuel penetration height.

Fig. 5 shows the predicted recirculation zone equivalence ratio as a function of fuel penetration height obtained from the parametric study. Of particular interest is the result for near-zero penetration height,  $\ell/r_0 \approx 0$ . Under this condition, for a global equivalence ratio of unity, the predicted recirculation zone fuel/air ratio is extremely fuel-rich, with  $\phi_{RZ} = 4.5$ . These high values of equivalence ratio produce a substantially cooler recirculation region than would be obtained for conditions nearer stoichiometric, and this in turn leads to reduced flame propagation rates and lower overall combustion efficiency in the combustor. Evaluation of the effect of the rich fuel/air ratio in the recirculation zone on overall performance is, however, complicated by difficulties that are encountered in modeling chemical kinetics in very fuel-rich regions.

There is no currently available finite-rate chemical kinetics model which can provide adequate results for complex hydrocarbon fuels under fuel-rich conditions, at temperatures at which the effects of dissociation manifest themselves. The modular model formulation used for the computations described in this paper includes as options either a one-step finite-rate model (Ref. 4) or the quasiglobal kinetics model (Refs. 2, 14). In the former case, the products of combustion are the fully-reacted species  $H_2O$  and  $CO_2$ , so that the effects of dissociation are ignored, and the overall reaction rate is underpredicted. The quasiglobal model used in the modular formulation is valid for complex hydrocarbon fuels and includes the effects of dissociation, but is not appropriate for equivalence ratios much above stoichiometric. Other models have been proposed for fuel-rich conditions, such as the four-step model of Dryer and Glassman, Ref. 12, but this model ignores dissociation

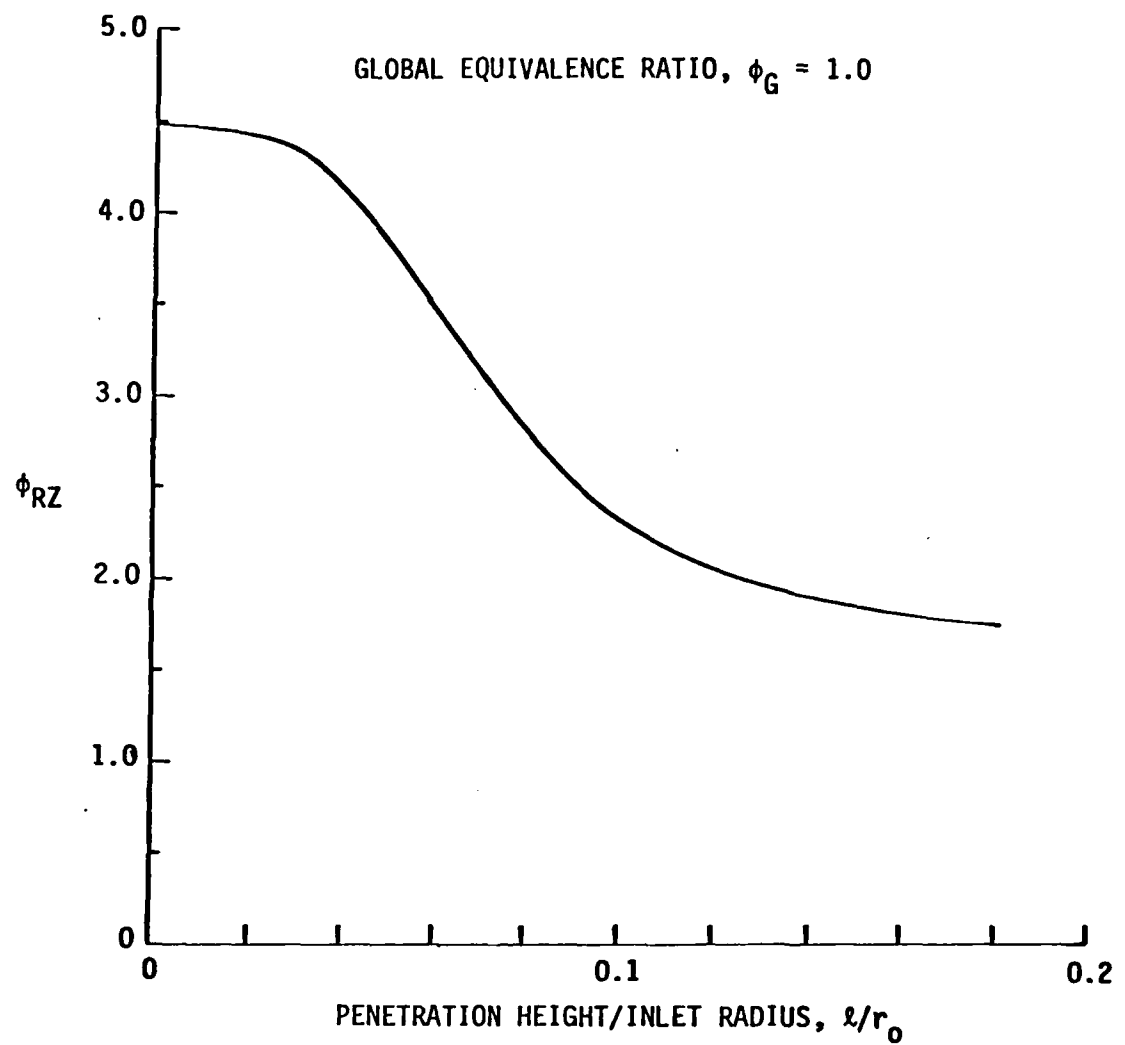


FIGURE 5. Recirculation Zone Equivalence Ratio as a Function of Penetration Height

effects. Thus it is difficult to obtain reliable estimates for the chemical kinetic rates that pertain in combustors in which significant regions of the flowfield are highly fuel-rich.

This difficulty is reflected in the performance results shown in Fig. 6. While the trend of combustion efficiency as a function of fuel penetration distance obtained through the use of the one-step global kinetics model is as expected, the magnitude of the overall change is relatively small and probably incorrect. The reason that the magnitude of these results can be expected to be incorrect is that the global finite-rate model can be expected to significantly overpredict the recirculation zone temperature for fuel-rich conditions, since the only effect of fuel-rich operation that this model recognizes is a dilution of the products of combustion with excess fuel for  $\phi \gg 1$ . With this model, the reaction rate is linear with respect to fuel concentration, whereas evidence exists that for fuel-rich conditions reaction rates do not continue to increase with fuel concentration, and, as noted earlier, dissociation effects are also ignored.

Nevertheless these results indicate that for the conditions considered, low values of fuel penetration distance are directly coupled to reductions in overall combustor performance. Since further development testing using fuel injection schemes designed to increase fuel penetration resulted in substantial performance improvements, it can be considered that the trends demonstrated by this modeling effort have been experimentally verified.

In the descriptions of the modular approach to the development of combustor models outlined in Refs. 1, 4, 6 and 7 it has been stressed that one of the features of the modular approach is that each of the elements involved in the overall combustor model can be independently developed. Just such an approach is being followed at SAI where, under a DOE-sponsored program, the extension of the quasiglobal model to fuel-rich conditions is being explored using the well-stirred reactor element of the model. One result of this work is shown in Fig. 7, on which predictions using several different kinetics models are compared to measured temperature data obtained in a laboratory well-stirred reactor burning toluene under both fuel-lean and fuel-rich conditions. All of these results are for the same stirred reactor residence time. For the fuel-rich condition, Fig. 7 shows that the extended quasiglobal model

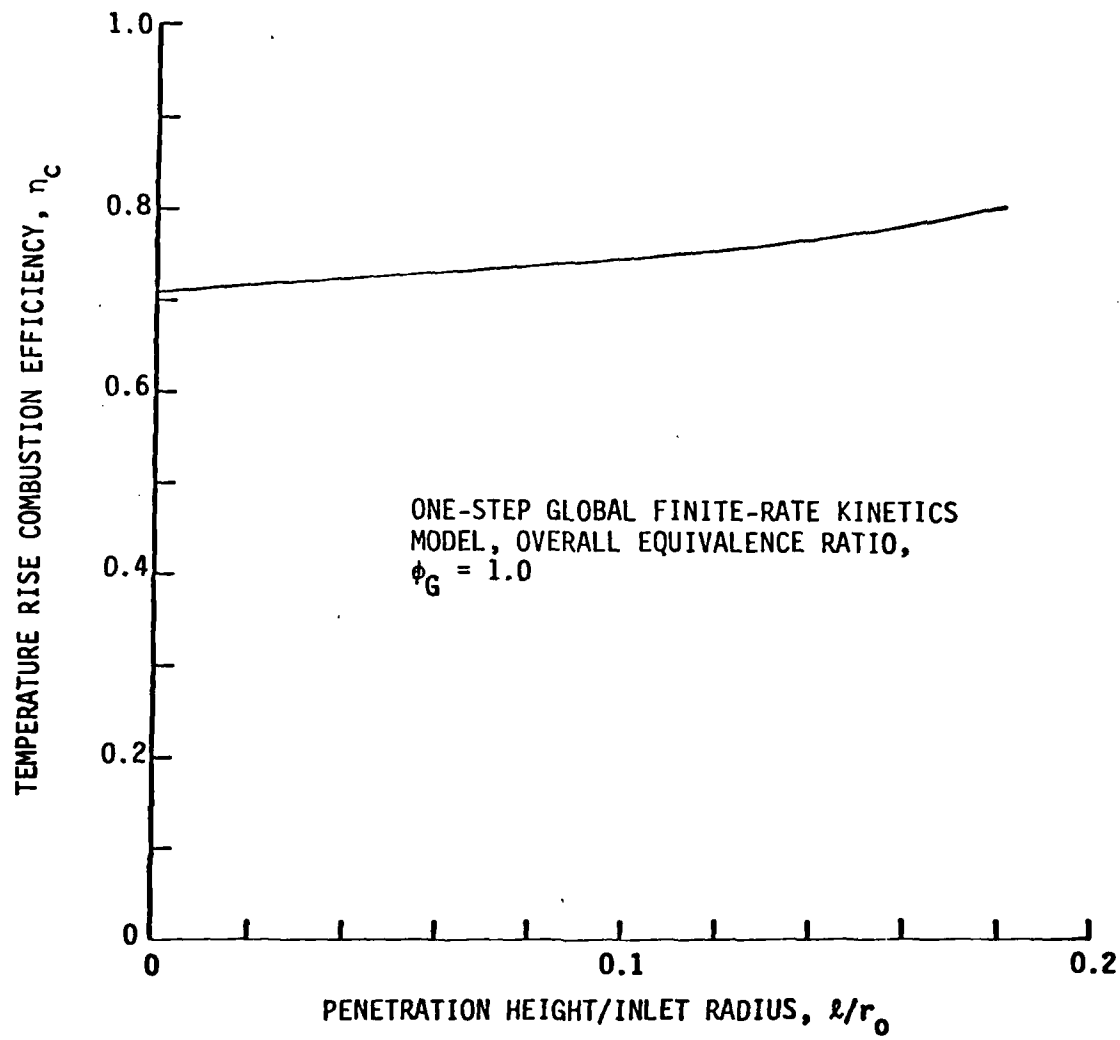


FIGURE 6. Predicted overall combustion efficiency as a function of fuel penetration height.

substantially improves the stirred reactor temperature prediction as compared to either the original quasiglobal formulation (Refs. 2, 11) or the four-step model (Ref. 12).

Although the extended quasiglobal formulation has not yet been fully developed, an indication of the effect of using this approach in a combustor calculation is demonstrated by Fig. 8, which shows recirculation zone temperatures for the conditions of the preceding section, computed using the four-step model (Ref. 12), the one-step model (Ref. 4), and the extended quasiglobal formulation (Ref. 13). While these results are provisional in that the extended quasiglobal model has not at this point been verified for ramjet fuels or operating conditions, they indicate a significant effect on recirculation zone temperature. In particular, at  $\phi_{RZ} = 3.0$ , the recirculation zone temperature predicted using the extended quasiglobal model is some 300°K lower than that obtained from the one-step model. This difference, coupled with the radically different species distributions obtained from the two models, can be expected to exert a significant influence on predicted flame propagation rates.

In summary, a comparison of modular model predictions with available data shows that the model is capable of predicting both the entrainment rate into sudden-expansion combustor recirculation regions and the overall fuel/air ratio in these regions. Both of these parameters are crucial to investigations of flame stability in a liquid fueled sudden-expansion combustor. An application of the approach in the interpretation of ramjet combustor test data has also been demonstrated: This demonstration shows that the model provides a means of verifying suspected causes of combustor performance deficiencies. The inadequacy of current chemical kinetics models under very fuel-rich conditions in circumstances under which the effects of dissociation are apparent provides a current limitation on the use of the modular model approach. However, related chemical kinetic model development work which can remove this limitation has been described.

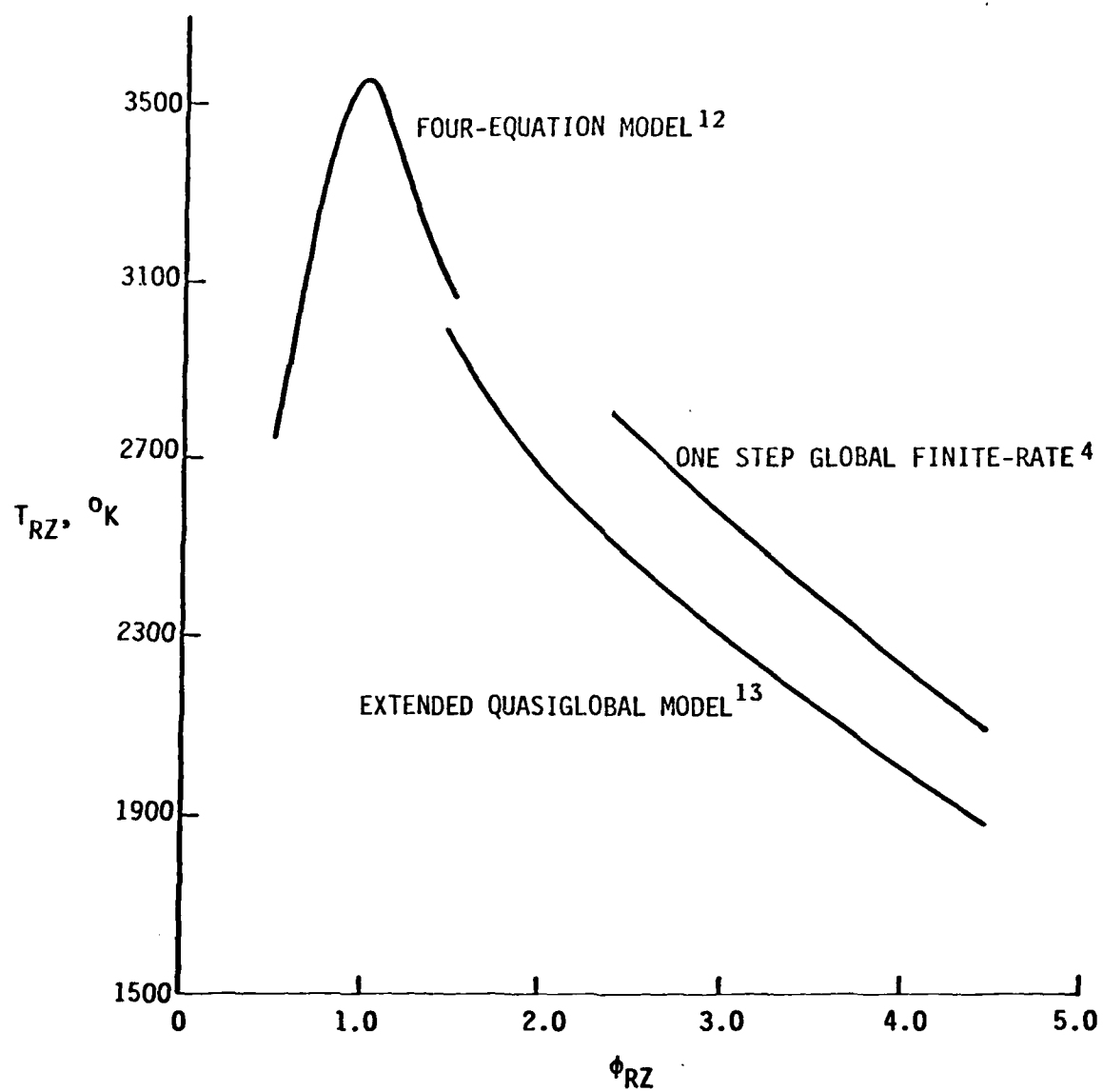


FIGURE 8. Combustor recirculation zone temperatures computed using different chemistry models.

### 3. MODIFICATIONS TO MODULAR MODEL FOR BORON SLURRY FUEL COMBUSTION

Boron slurry fuels have a high energy density and are therefore extremely attractive for volume-limited ramjet applications. However, the advantages of boron slurry fuels are only available if combustion efficiencies comparable to those obtained with more conventional hydrocarbon fuels can be attained. In past combustor development work the realization of high levels of combustion efficiency has been achieved only at the cost of large total pressure losses in the combustor, which forces unacceptable design compromises.

Because the mechanisms involved in boron slurry combustion are considerably different from those involved in the combustion of liquid hydrocarbon fuels, the empirical design guidelines that have been developed for conventional fuels do not apply. Even for conventional fuels, the need for reduced combustor volume and the packaging requirements that lead to the use of a sudden-expansion dump combustor have together reduced the applicability of empirical design and scaling rules. For this reason, an analytical tool for the design and scaling of sudden-expansion ramjet combustors, utilizing conventional hydrocarbon fuels has been developed and tested, as outlined in the preceding section. This code combines a semi-empirical analysis of the fuel injection processes with a sophisticated turbulent kinetic energy analysis of the mixing process and a quasiglobal finite-rate hydrocarbon chemical kinetics mechanism in an iterative analysis of a sudden-expansion combustor with large scale embedded recirculation zones. Because of current interest in boron slurry fuels for ramjets and the inapplicability of empirical guidelines for the design of ramjet combustors using these fuels, the development of a further modification to the modular model for liquid-fueled sudden-expansion ramjets, to extend the approach to boron fuel combustion, has been initiated under this AFOSR program.

Boron slurry fuel combustion is a complex phenomenon involving two-phase flow and finite-rate reaction processes in the gas phase and on the particle surface. The boron is generally in the form of micron-size particles suspended in a carrier hydrocarbon fuel. One of the difficulties involved in boron combustion is that a surface oxide layer can form on the particle. This oxide has a boiling point below that of the metal, so that the boron combustion

process involves a diffusion of oxidizing gases through the oxide layer with a surface reaction mechanism involved at the particle surface. Since this is a relatively slow process, one strategy for obtaining high boron combustion efficiencies is to limit the amount of oxygen reaching the surface of the particle during the heat-up of the particle, i.e., carrying out the particle heat-up in a regime which is fuel-rich relative to the hydrocarbon carrier, and then exposing the hot particles and remaining fuel to additional air. This form of staged combustion is difficult to achieve in practice, and the assembly of a computer analysis to aid in achieving it is one of the goals of this task.

The analysis of the combustion of a boron slurry fuel in a ramjet combustor begins just downstream of the point of injection of the fuel. A spray is formed, which involves a distribution of droplet sizes within which there is also a distribution of boron particle sizes. As the fuel evaporates and burns, there remains a cloud of boron particles, with varying sizes and varying oxide layer thicknesses. To compute the subsequent fate of these particles in the combustor, it can be assumed that the particles are in near dynamic equilibrium, which means that, with respect to the mean velocity in the combustor, the particles follow the gas phase, but they do not necessarily follow the turbulent fluctuations of the gas phase. Thus there is an effective diffusion of particles relative to the gas phase.

In the analysis, the continuous distribution of particles is discretized into a number of classes, with the class described by an average particle size and oxide layer thickness range. It is further assumed that these particles form a dilute continuum, so that the motion of each class can be described by a species transport equation and the thermal history of each class by a particulate energy equation. The coupling of these species and energy equations to the gas phase combustion and heat transfer mechanisms is through source terms which model the rate of consumption and heat transfer phenomena for each class of particles. Since the boron oxidation process is in general occurring simultaneously with the oxidation of the hydrocarbon carrier fuel, these chemical kinetic phenomena must be considered together, which requires the addition of species involved in the boron oxidation process to those already included in the model.

The two major modifications to the modular model that are required for the modeling of boron slurry combustion are the development and introduction of a particle-tracking methodology and the development and introduction of submodels for the boron particle heat-up and combustion processes. These two modifications are the subject of this Section. As there currently exists no comprehensive model for boron particle combustion, the two most complete models available have been coded as interchangeable subroutines which, in addition to their use within the modular model, can also be utilized as single-particle models. In the latter mode, these subroutines can be used in the development of more complete models of the boron combustion process, through comparison of single-particle model results with relevant experimental data. The particle tracking formalism has been incorporated into the code utilizing a total of ten particle categories: as each additional category involves an additional species transport equation, in addition to an increase in the overall storage required for the code, ten categories have been selected as providing the best balance between the need for discrimination of particle size effects and the overall code run time required for solution.

### 3.1 BORON IGNITION AND COMBUSTION MODELS

There are a number of models for the ignition and combustion of single particles of boron. A variety of these have been investigated for possible application in the modular model for slurry-fueled ramjets, including those reported by King (Refs. 14, 15), Meese (Ref. 16), Vovchuck (Ref. 17), Mohan (Ref. 18) and Edelman (Refs. 19, 20). The component equations used in each of these models are summarized in Table 1, which also incorporates the assumptions built into the models; the nomenclature for Table 1 is given in Table 2.

In reviewing these models, the emphasis has in each case been on the utility and generality of the approach with respect to the question of addressing the combustion of boron particles under the wide range of conditions appropriate to ramjet operation. The attention given to both diffusion controlled and kinetically controlled mechanisms was examined, as was the characterization (if any) of oxide removal by water.

In general, the formulations are based upon the conservation equations for mass and energy. The momentum equation is not explicitly coupled into the equation set but in certain of the models the relative velocity effect is accounted for through a Nusselt number correction on heat and mass transfer. In most of the formulations the energy equation is the central element of the model, with the size history and other transport relationships representing auxiliary elements of the model.

King considers three intervals in the heat-up of the particle: below phase change of the boron, at phase change of the boron, and above the phase change of the boron (melting point 2450°K). Meese, who based his work on a 1972 paper of King's, also includes the boil-off of the oxide layer. For conduction, King assumes the particle moves at the velocity of the surrounding gas, whereas Meese allows for the incorporation in his calculation of the convective heat-transfer coefficient. Vovchuk includes no convective heat transfer and in Table 1, this section for Vovchuk is omitted. This is the form used when a section does not apply to an author's work. Edelman also allows for convective heat transfer. The format for the listing of the radiation component in Table 1 is the same as that used for the convection terms. Each radiation equation could be interchanged with the other radiation equations with only minor modifications to match an author's model (i.e. volume based on a slab or a particle). It should be noted that Vovchuk includes a radiation term which he eventually neglects.

For oxide formation, King, Meese, and Mohan use the global reaction  $B + 3/4O_2 \rightarrow 1/2B_2O_3$ . Vovchuk allows for lower oxides  $BO$ ,  $BO_2$ ,  $B_2O_2$ , forming at the surface. Edelman includes  $BO$  with  $B_2O_3$  but if  $BO$  forms it does not oxidize further. All reactions are diffusion controlled for the first four authors and kinetics controls the reactions Edelman uses.

For oxide consumption, only King and Meese consider the chemical effect of water on boric oxide ( $B_2O_3 + H_2O \rightarrow 2HBO_2$ ). The only other mechanism considered for oxide removal is evaporation.

Diffusion equations in King's work are algebraic in form and depend upon absolute values of pressures at infinity and the surface. Vovchuk integrates the partial pressure from the surface to infinity. For diffusion through the oxide layer King and Meese have similar equations that vary only in one constant.

Meese's constant was derived from data unavailable to King and fits the data curve better.

A major part of King's model is the phase change of the boron. Meese has a similar equation though derived in a slightly different fashion. Edelman assumes a finite evaporation rate of the boron. For evaporation of the oxide King and Meese are again similar. Vovchuk and Edelman have no oxide layer to remove. Mohan's phase change model, instead of being equilibrium controlled, is finite rate.

Edelman is the only author who includes finite rate kinetics. He assumes the particle has ignited and studies surface oxidation kinetics. Vovchuk also studies only combustion in the diffusion controlled mode.

The Nusselt number correlation allows for the effect of a velocity difference on convective heat transfer. King sets the value of two ( $N_u = 2$ ) by assuming a zero velocity difference. Meese and Edelman allow for variation in velocities.

In Meese's model nothing else occurs while the oxide layer boils off leading to an independent expression for the oil off time. The end product of Vovchuk's work is, the burning time. Mohan also derived an expression for the burning time. The radius and, in cases where the oxide is considered, the oxide layer thickness equation are basic to all but Vovchuk's model.

Three of the models consider ignition: King, Meese, and Mohan. They all essentially take it to be the point where the oxide layer boils or flashes off. Other assumptions and restrictions made by each author appear at the end of Table 1.

Based upon this review and formulation, the two most promising models for use in ramjet applications are those of King and Edelman. These are most general in their respective formulations; the others are either derivatives of them or are too restrictive to be usefully extended.

### 3.2 BORON PARTICLE COMBUSTION SUBROUTINES FOR THE MODULAR MODEL

The emphasis in this phase of the present work was on the creation of a single-particle combustion code which could employ either the methodology of King (Refs. 14, 15) or that employed by Edelman (Refs. 19, 20). The concept

TABLE 1. Summary of Available Boron Ignition and Combustion Models.

COMPLETE HEAT TRANSFER EQUATIONS	$\left( \frac{4}{3} \times r_p^3 \rho_B c_{PB} (\text{S or L}) + 4 \times r_p^2 X \rho_{B_2O_3} c_{PB_2O_3} \right) \frac{dT_p}{dt} = R_B (Q_{RX}) - R_E (\Delta H_{VAP}) - R_H \Delta H_H + 4 \times (r_p + X)^2 \cdot [h (T_m - T_p) + \alpha \epsilon \alpha_R (T_{RAD}^* - T_p^*)]$	King
	$(m_B c_{PB} + m_{B_2O_3} c_{PB_2O_3}) \frac{dT_p}{dt} = R_Q - R_E \Delta H_{VAP} + 4 \times r_2^2 \cdot [h (T_g - T_p) + \alpha \epsilon \alpha (T_{RAD}^* - T_p^*)]$	Meese
	$-4 \times \lambda r^2 \frac{dT}{dr} = I_{O_2} H_{O_2}(T) + I_B H_B(T_k) - I_{B_2} H_{B_2O_3}(T) - Q_R^K$	Vovchuk
	$h \rho_C c_C \frac{dT_C}{dt} = q_B \rho_B R_B - q_C \rho_C R_C - L$	Mohan
HEAT TRANSFER: CONDUCTION-CONVECTION COMPONENTS	$\frac{dT_p}{dt} = \frac{3}{2} \frac{\alpha \lambda (\text{Nu})}{\delta_s c_{ps} R^2 c_p} + \left\{ \frac{c_p (T_g - T_p)}{e^R - 1} - L + A k_s \left[ \frac{2 c_p \rho_s R}{\alpha \lambda (\text{Nu}) y_{O_2,s}} \right] + \frac{M_B}{M_{O_2}} \Delta H_R - \frac{2 \alpha \epsilon R c_p}{\alpha \lambda (\text{Nu})} (T_p^* - T_w) \right\}$	Edelman
	① $\left( \frac{4}{3} \times r_p^3 \rho_B c_{PB,S} + 4 \times r_p^2 X \rho_{B_2O_3} c_{PB_2O_3} \right) \frac{dT_p}{dt} = 4 \times (r_p + X)^2 (T_m - T_p) h$ BELOW PHASE CHANGE OF BORON, $T_p < 2450$	King
	② $\left( \frac{4}{3} \times r_p^3 \rho_B \Delta H_m \right) \frac{df}{dt} = 4 \times (r_p + X)^2 (T_m - T_p) h$ AT PHASE CHANGE, $T_p = 2450$ , $0 < f < 1$	King
	③ $\left( \frac{4}{3} \times r_p^3 \rho_B c_{PB,L} + 4 \times r_p^2 X \rho_{B_2O_3} c_{PB_2O_3} \right) \frac{dT_p}{dt} = 4 \times (r_p + X)^2 (T_m - T_p) h$ ABOVE PHASE CHANGE, $T_p > 2450$ , $f = 1$	King
	$(m_B c_{PB} + m_{B_2O_3} c_{PB_2O_3}) \frac{dT_p}{dt} = 4 \times r_2^2 h (T_g - T_p)$	Meese
	$h \rho_C c_C \frac{dT_C}{dt} = (T_C - T) \frac{2\lambda}{R}$	Mohan
HEAT TRANSFER: RADIATION	$\frac{4}{3} \times R^3 \delta_s c_{ps} \frac{dT}{dt} = 4 \times R^2 h (T_g - T_p) \frac{\alpha}{e^R - 1}$	Edelman
	① $\left( \frac{4}{3} \times r_p^3 \rho_B c_{PB,S} + 4 \times r_p^2 X \rho_{B_2O_3} c_{PB_2O_3} \right) \frac{dT_p}{dt} = 4 \times (r_p + X)^2 \alpha \epsilon \alpha_R (T_{RAD}^* - T_p^*)$	King
	② $\left( \frac{4}{3} \times r_p^3 \rho_B \Delta H_m \right) \frac{df}{dt} = 4 \times (r_p + X)^2 \alpha \epsilon \alpha_R (T_{RAD}^* - T_p^*)$	King
	③ $\left( \frac{4}{3} \times r_p^3 \rho_B c_{PB,L} + 4 \times r_p^2 X \rho_{B_2O_3} c_{PB_2O_3} \right) \frac{dT_p}{dt} = 4 \times (r_p + X)^2 \alpha \epsilon \alpha_R (T_{RAD}^* - T_p^*)$	King
	$(m_B c_{PB} + m_{B_2O_3} c_{PB_2O_3}) \frac{dT_p}{dt} = 4 \times r_2^2 \alpha \epsilon \alpha (T_{RAD}^* - T_p^*)$	Meese
	$-4 \times \lambda r^2 \frac{dT}{dr} = -4 \times r_2^2 \epsilon \alpha (T_k^* - T)$	Vovchuk

HEAT TRANSFER: RADIATION	$\hbar \rho_c c_c \frac{dT_c}{dt} = -1.36 \times \left(\frac{T_c}{1000}\right)^n$	Mohan
	$\frac{4}{3} \times R^2 c_{ps} \epsilon_s \frac{dT_p}{dt} = 4 \times R^2 \sigma \epsilon (T_p^4 - T_w^4)$	Edelman
OXIDE FORMATION	$B(s, t) + \frac{3}{4} O_2(g) \rightarrow \frac{1}{2} B_2O_3(g)$ FAST REACTION DIFFUSION LIMITED HAPPENS AT OXIDE-BORON INTERFACE	King
	$B(s, t) + \frac{3}{4} O_2(g) \rightarrow \frac{1}{2} B_2O_3(g)$ WORK BASED ON KING'S	Meese
	$2B_2O_2(g) \rightleftharpoons B_2O_3(g) + \frac{1}{2} O_2(g)$ THERMAL EQUILIBRIUM $B_2O_3(g) \rightleftharpoons 2B_2O(g) + \frac{1}{2} O_2(g)$ DIFFUSION CONTROLLED LOWER OXIDES ONLY AT SURFACE $B_2O_2(g) \rightleftharpoons 2B_2O(g)$	Vovchuk
OXIDE CONSUMPTION	$B(s) + \frac{3}{4} O_2(g) \rightarrow \frac{1}{2} B_2O_3(l)$ DIFFUSION CONTROLLED EQUILIBRIUM VAPORIZATION OF $B_2O_3$ AND ABSORPTION OF $O_2$ IN THE LIQUID $B_2O_3$ AT LIQUID-GAS SURFACE.	Mohan
	$B(l) + \frac{1}{2} O_2(g) \rightarrow BO(g)$ FINITE-RATE KINETICS CONTROLLED $B(l) + \frac{3}{4} O_2(g) \rightarrow \frac{1}{2} B_2O_3(g)$	Edelman
	$H_2O(g) + B_2O_3(l) \rightarrow 2HBO_2(g)$ DIFFUSION LIMITED ENDOTHERMIC REACTION RATE CONTROLLED EVAPORATION	King
DIFFUSION THROUGH GAS FILM	$H_2O(g) + B_2O_3(l) \rightarrow 2HBO_2(g)$ WORK BASED ON KING'S	Meese
	DIFFUSIVITY OF $B_2O_3$ , $HBO_2$ , $H_2O$ GAS THROUGH $N_2$ FILM; $J = \text{ONE OF: } B_2O_3, HBO_2, H_2O$ $D_{J, N_2} = 4.3 \times 10^{-8} \times \frac{T_p^{1/4}}{P(V_J^{1/2} + V_{N_2}^{1/2})} \sqrt{\frac{1}{(MW)_J} + \frac{1}{(MW)_{N_2}}}$	King
	$R_H = \frac{D_{H_2O, N_2} \text{MW}}{4 \times (r_p + x)^2 \times 2(r_p + x) R T_p} (P_{H_2O, \text{SURF}} - P_{H_2O, \text{SURF}})$ $R_H = \frac{D_{HBO_2, N_2} \text{MW}}{4 \times (r_p + x)^2 \times 4(r_p + x) R T_p} (P_{HBO_2, \text{SURF}})$ MOLAR REMOVAL RATE OF OXIDE BY WATER	
RATES AND CONSTANTS	WORK BASED ON KING'S	Meese
	$I_{O_2} = -4 \times r^2 \frac{D}{RT} \frac{dP_{O_2}}{dr} ; I_{BO} = -4 \times r^2 \frac{D}{RT} \frac{dP_{BO}}{dr}$ ETC. $B_2O_2$ , $B_2O_3$ , $BO_2$	Vovchuk
	$R_c = 2 X_a D_a P_a / \rho_c d$ OUTWARD GAS-PHASE DIFFUSION OF $B_2O_3$ $R_b = R_c = (q_c \rho_c R_c + L) / q_b \rho_b$ AT LOW TEMP. STAGE	Mohan
	KINETICALLY CONTROLLED	Edelman

	$R_B = \frac{4 \pi (r_p + x)^2 k_1 e^{-k/T_p} (P_{O_2}) T_p}{x}$ $R_B = \frac{64.8 \cdot 10^{-6} (r_p + x)^2 T_p e^{-12000/T_p} (P_{O_2, SURF})}{x}$	MOLAR CONSUMPTION RATE OF BORON $\frac{3}{4} O_2$ to 1 B	King
DIFFUSION THROUGH OXIDE LAYER	$R = \frac{1}{\Delta r} 2.0 \cdot 10^{-6} r_2^2 T_p P_{O_2} \exp(-12000/T_p)$ ONLY CHANGE FROM KING'S		Meese
	NO OXIDE LAYER		Vovchuk
	$R_B = X k D / h$		Mohan
	NO OXIDE LAYER		Edelman
PHASE CHANGE BORON	$\frac{df}{d\theta} = \text{Z of } B(L) = \frac{R_B(Q_{RX}) - R_E(\Delta H_{VAP}) - R_H \Delta H_H + 4\pi(r_p + x)^2 \left[ h(T_m - T_p) + \alpha \epsilon \alpha_R (T_{RAD}^* - T_p^*) \right]}{\frac{4}{3} \pi r_p^3 \rho_B \Delta H_m}$		King
	$\Delta H_f \frac{m_B}{H_B} \int_0^{t_n} dt \left\{ R_Q - R_E \Delta H_{VAP} + 4\pi r_1^2 [h(T_m - T_p) + \alpha \epsilon \alpha (T_{RAD}^* - T_p^*)] \right\}$		Meese
	$\dot{n}_T = \frac{4\pi R^2 \alpha}{\sqrt{2\pi M_B R_0 T_p}} [P_{V,B}(T_p) - P_{B,S}]$		Edelman
PHASE CHANGE OXIDE	$R_E = \frac{1.005 \cdot 10^{10} (r_p + x)^2 \alpha e^{-12000/T_p}}{T_p^2 \left\{ 1 + [(4.5 \cdot 10^7) \alpha P (r_p + x) / T_p (\text{Nu})] \right\}}$ MOLAR EVAPORATION RATE OF $B_2O_3$		King
	$R_E = 1.225 \cdot 10^6 r_2^2 \exp(-42000/T_p)$		Meese
	NO OXIDE LAYER		Vovchuk
	$\frac{R_c}{R_V} = 2 D_a / d C \alpha$ LIMITED DEPENDING ON $\alpha$		Mohan
	NO OXIDE LAYER		Edelman
CHEMISTRY	$H_2O(g) + B_2O_3(s) \rightarrow 2HBO_2(g)$	$B(s,s) + \frac{3}{4} O_2(g) \rightarrow \frac{1}{2} B_2O_3(g)$	King
	$H_2O(g) + B_2O_3(s) \rightarrow 2HBO_2(g)$	$B(s,s) + \frac{3}{4} O_2(g) \rightarrow \frac{1}{2} B_2O_3(s,g)$	Meese
	$2B_2O_2(g) \rightleftharpoons B_2O_3(g) + \frac{1}{2} O_2(g)$		Vovchuk
	$B_2O_3(g) \rightleftharpoons 2BO(g) + \frac{1}{2} O_2(g)$		
	$B_2O_2(g) \rightleftharpoons 2BO(g)$		
	$B(s) + \frac{3}{4} O_2(g) \rightarrow \frac{1}{2} B_2O_3(s)$	$B_2O_2(g) + \frac{1}{2} O_2(g) \rightarrow B_2O_3(g)$	Mohan
CHEMICAL KINETICS	$B(s) + \frac{1}{2} O(g) \rightarrow BO(g)$	$B(s) + \frac{3}{4} O_2(g) \rightarrow B_2O_3(g)$	Edelman
	$a_c = A k_s \frac{N_B}{K_{O_2}} P_s y_{O_2,s} \left( \frac{R c_{ps}}{1(\text{Nu}/2)} \right)$		Edelman

SPECIES FOUND AT THE SURFACE	$H_2O(g)$ , $HBO_2(g)$ , $O_2(g)$ , $B_2O_3(l,g)$ , $B(s,l)$ , $N_2(g)$	King
	$H_2O(g)$ , $HBO_2(g)$ , $O_2(g)$ , $B_2O_3(l,g)$ , $B(s,l)$ , $N_2(g)$	Meese
	$B(s,l)$ , $BO(g)$ , $BO_2(g)$ , $B_2O_2(g)$ , $B_2O_3(g)$ , $O_2(g)$	Vovchuk
	$B(s)$ , $B_2O_2(g)$ , $O_2(g)$ , $B_2O_3(l,g)$	Mohan
	$B(s,l)$ , $B_2O_2(g)$ , $O_2(g)$ , $N_2(g)$ , $BO(g)$	Edelman
SPECIES FOUND OFF SURFACE (GASES)	$HBO_2$ , $B_2O_3$ , $O_2$ , $H_2O$ , $N_2$	King
	$HBO_2$ , $B_2O_3$ , $O_2$ , $H_2O$ , $N_2$	Meese
	$B_2O_3$ , $B_2O_2$ , $O_2$	Vovchuk
	$B_2O_3$ , $N_2$ , $O_2$	Mohan
	$B_2O_3$ , $O_2$ , $N_2$ , $BO$	Edelman
MUSSELT NUMBER	SET EQUAL TO 2.0	King
	$(1 + 0.296 Pr^{1/3} Re^{1/2}) = Nu$ BASED ON RADIUS	Meese
	$Nu = 2 + 0.276 Pr^{1/3} Re^{1/2}$	Edelman
	$Pr = \frac{c_p u_g}{\lambda}$ $Re = \frac{2 R \rho_g (v_g - v_p)}{u_g}$	
	BOIL-OFF TIME OF OXIDE LAYER	
BURNING TIMES	$t_B = \frac{\rho_{B_2O_3} (r_2^4 - r_1^4) \Delta H_{VAP}}{3r_2^2 (R/A) Q + h(T_g - T_p) + \alpha \sigma c (T_{RAD}^4 - T_p^4) M_{B_2O_3}}$	Meese
	$\tau_c = \frac{\rho_B d_{k0}^2}{16 u_B \frac{\bar{D}}{RT} \rho_{O_2}}$ $\tau_r = \frac{\rho_B d_{k0}^2}{8 u_B \frac{V_B}{V_{O_2}} \frac{P}{R} \frac{\bar{D}}{T} \left( \frac{1}{1 - \frac{V_{B_2O_3}}{V_{O_2}}} \right) \ln \left[ P - (1 - \frac{V_{B_2O_3}}{V_{O_2}}) \rho_{O_2} \right]}$	Vovchuk
	DROPLET COMBUSTION TIME	
	$t_B = \frac{c_p \rho_B d^2}{8A} \left\{ \ln \left[ 1 + \frac{Qy + c_p (T_m - T_L)}{A} \right] \right\}^{-1}$	Mohan
	$\frac{dr_B}{dt} = \frac{-R_B (MW)_B}{4 \pi r_p^2 \rho_B}$ $\frac{dx}{dt} = \frac{(R_B/2 - R_E - R_H)(MW)_{B_2O_3}}{4 \pi r_p^2 \rho_{B_2O_3}}$	King
RADIUS CHANGE AND/OR OXIDE CHANGE	$\frac{dm_B}{dt} = -R_B \rho_B$ $r_B = \frac{4}{3} \pi r_1^3 \rho_B$ $\frac{dm_{B_2O_3}}{dt} = (R/2 - R_E) \rho_{B_2O_3}$ $m_{B_2O_3} = \frac{4}{3} \pi (r_2^3 - r_1^3) \rho_{B_2O_3}$	Meese
	$\frac{dh}{dt} = R_B - R_C$ $R_B = X k D / n$ $R_C = 2 X_a D_a \rho_a / \rho_c d$	Mohan
	$\frac{d(R^2)}{dt} = \frac{-a \lambda (Nu)}{6 s c_p}$	Edelman

	<p><math>R_B</math> eq. includes: an Arrhenius viscosity-temperature law, <math>\kappa \sim A e^{-E/RT}</math>      Henry's law, <math>P_1/X_1 = K_1</math>      Wilke correlation, <math>D_{AB}^* = 7.4 \cdot 10^{-6} \frac{(\rho_m)_B^{1/2} T}{\eta_B V_A^{1/2}}</math></p>	King
EQUATION REFERENCES	<p><math>\sigma</math> Stefan's constant = <math>5.669 \cdot 10^{-8} \text{ W/m}^2 \text{ }^0\text{K} = 0.1714 \cdot 10^{-8} \text{ BTU/h-ft}^2 \text{ }^0\text{R}^4</math>  <math>D = D_0 (T/T_0)^{1.78}</math>      <math>\lambda = \lambda_0 (T/T_0)^{0.78}</math></p>	Vovchuk
	$R_B = X K D / h$ $P_e = \exp (H/R^0 T_B - H/R^0 T_c)$ KD can be expressed in an Arrhenius form (see King)	Mohan
	Clausius - Claperyon $\frac{d \ln P_S}{dt} = \frac{L_s}{RT^2}$	Edelman
EQUATIONS FOR $h$	$h = 0.347 \cdot 10^{-6} (\text{Nu}) T_m^{0.8} / (r_p + X)$ (1974) $h = 0.694 \cdot 10^{-6} T_m^{0.8} / r_2$ (1972)	King
	$h = (1 + 0.296 \text{ Pr}^{1/4} \text{ Re}^{1/2}) k_g/r$	Meese
IGNITION	<p>The first stage of a two stage burn. During this time the oxide layer is removed.</p> <p>A state at which no energy barriers stand between that state and steady-state combustion.</p> <p>Only considers combustion.</p> <p>Similar to King's.</p> <p>N/A</p>	King Meese Vovchuk Mohan Edelman
	<p>Oxide generation controlled by diffusion of oxygen through liquid oxide layer.      Uniform particle temperature.      Vaporization and diffusion considered as series resistances.  <math>H_2O</math> removes <math>B_2O_3</math> by diffusion limited reaction (endothermic).      Heat gain/loss by convection, radiation.      Partial pressure of <math>HBO_2</math> negligible in the free stream.      Particle is stationary with respect to surrounding gasses.      Paper only deals with ignition.</p>	King
ASSUMPTIONS	<p>Initial <math>B_2O_3</math> layer thickness is uniform.      Uniform particle temperature.      The convective heat transfer coefficient, <math>h</math>, is known.      Surroundings treated as black at temperature <math>T_{RAD}</math>.      Prior to oxide removal, boron reaction rate is diffusion controlled and forms <math>B_2O_3</math>.  <math>B_2O_3</math> evaporation follows an Arrhenius type relation.      Particle temperature remains constant during melting and boiling.      Variation in <math>h</math>, surface reaction rate and oxide evaporation rate are neglected during oxide boiling.      Water vapor reduces the activation energy of oxide evaporation.      Initial particle temperature is below oxide boiling and boron melting.  <math>B_2O_3</math> formed during boiling may be neglected.      No net radiative exchange between particle and cloud.      Convective heat transfer neglected in final computations.</p> <p>The particle has been heated to equilibrium temperature.      Reaction occurs at the surface.      The diffusion coefficients for the oxidant and reaction products are identical.      Radiation can be neglected to a first approximation (<math>d \leq 100 \mu m</math>).      Particle temperature is above oxide boiling and boron melting points.</p> <p>Diffusion controlled <math>B + 3/4 O_2 \rightarrow 1/2 B_2O_3</math>.      Liquid layer is isothermal.      Ideal gas.      Absorptive equilibrium for <math>O_2</math> at C and 1D steady-state diffusion of <math>O_2</math> within liquid layer.      Plane two-dimensional slab model.</p> <p>No oxide layer.      Uniform particle temperature.      Surface combustion kinetics.      Finite-rate evaporation of boron from the surface.</p>	Meese Vovchuk Mohan Edelman

TABLE 2. Nomenclature for Expressions Summarized in Table 1

2.1 King's Model

$C_{PB1}$	liquid boron heat capacity (cal/gm°K)
$C_{PBS}$	solid boron heat capacity (cal/gm°K)
$C_{B_2O_2}$	liquid boron oxide heat capacity (cal/gm°K)
$f$	fraction of boron in the liquid phase
$h$	gas-particle heat transfer coefficient (cal/cm <sup>2</sup> sec°K)
$k$	mass transfer coefficient for transport of boric oxide gas from particle to free-stream (gm-mol/cm <sup>2</sup> atm sec)
$(MW)_B$	boron atomic weight (gm/gm-mol)
$(MW)_{B_2O_2}$	boric oxide molecular weight (gm/gm-mol)
Nu	Nusselt Number
P	total pressure (atm)
$P_{O_2}$	oxygen partial pressure in free stream (atm)
$P_{B_2O_3, \text{surf}}$	boric oxide partial pressure adjacent to particle surface (atm)
$P_{B_2O_3}^{\circ}$	boric oxide vapor pressure (atm)
$P_{H_2O, \text{surf}}$	water gas partial pressure adjacent to particle surface (atm)
$P_{HBO_2, \text{surf}}$	$HBO_2$ partial pressure adjacent to particle surface (atm)
$P_{B_2O_3, \infty}$	boric oxide partial pressure in free-stream (atm)
$Q_{RX}$	heat release of $B(s) + \frac{3}{4}O_2 \rightarrow \frac{1}{2}B_2O_3(l)$ (cal/gm-mol)
$Q_{RX2}$	heat release of $B(l) + \frac{3}{4}O_2 \rightarrow \frac{1}{2}B_2O_3(l)$ (cal/gm-mol)
R	gas law constant, $82.06 \text{ atm-cm}^3/\text{gm-mol}^\circ\text{K}$
$R_B$	molar rate of boron consumption (gm-mol/sec)
$R_E$	molar evaporation rate of boric oxide (gm-mol/sec)
$R_H$	molar rate of removal of $B_2O_3$ by water reaction (gm-mol/sec)
$r_p$	boron particle radius (cm)
$T_{\infty}$	free stream gas temperature ( $^\circ\text{K}$ )
$T_{CL}$	particle center temperature ( $^\circ\text{K}$ )
$T_p$	particle temperature ( $^\circ\text{K}$ )
$T_{RAD}$	surroundings radiation temperature ( $^\circ\text{K}$ )

$T_s$	particle surface temperature ( $^{\circ}$ K)
$V_j$	molecular volume of species $j$ ( $\text{cm}^3$ )
$X$	oxide layer thickness (cm)
$D_{B_2O_3, N_2}$	diffusivity of gaseous boric oxide in nitrogen ( $\text{cm}^2/\text{sec}$ )
$D_{HBO_2, N_2}$	diffusivity of $HBO_2$ in nitrogen ( $\text{cm}^2/\text{sec}$ )
$D_{H_2O, N_2}$	diffusivity of water gas in nitrogen ( $\text{cm}^2/\text{sec}$ )
$\Delta H_H$	heat absorbed by reaction of $H_2O$ with $B_2O_3(l)$ (cal/gm-mol)
$\Delta H_m$	heat of fusion of boron (cal/gm)
$\Delta H_{VAP}$	heat of vaporization of $B_2O_3(l)$ (cal/gm-mol)
$\alpha$	evaporation coefficient of boric oxide liquid
$\alpha_R$	surroundings absorptivity
$\alpha_t$	thermal diffusivity of boron ( $\text{cm}^2/\text{sec}$ )
$\sigma$	Stefan-Boltzmann constant, $1.354 \cdot 10^{12}$ cal/ $\text{cm}^2\text{sec}^{\circ}\text{K}^4$
$\epsilon$	particle emissivity
$v$	Hertz-Knudsen impingement factor (gm-mol/ $\text{cm}^2\text{atm sec}$ )
$\theta$	time (sec)
$\rho_B$	boron density ( $\text{gm}/\text{cm}^3$ )
$\rho_{B_2O_3}$	boric oxide density ( $\text{gm}/\text{cm}^3$ )

## 2.2 Model of Meese and Skifstad

$A$	surface area, $\text{cm}^2$
$c_p$	specific heat, cal/g- $^{\circ}$ K
$d$	particle diameter, cm
$E$	activation energy for evaporation
$\Delta H_f$	heat of fusion of boron, cal/g
$\Delta H_{vap}$	heat of vaporization of boron oxide, cal/mole
$h$	convective heat-transfer coefficient, cal/ $\text{cm}^2\text{-sec-}^{\circ}\text{K}$
$k$	thermal conductivity, cal/cm-sec- $^{\circ}$ K
$M$	molecular weight, g/g-mole
$m$	mass, g
$P$	pressure, atm
$Pr$	Prandtl number of the gas
$Q$	heat of combustion of boron with diatomic oxygen to form liquid $B_2O_3$ , cal/mole; total energy, cal

R	molar rate of consumption of boron, g-mole/sec; gas constant
$R_E$	molar rate of evaporation of boron oxide, gm-mole/sec
Re	Reynolds number based on particle diameter and relative velocity between the gas and particle
r	radius, cm
$\Delta r$	oxide film thickness, $r_2 - r_1$ , cm
T	temperature, °K
t	time, sec
$x_{H_2O}$	mole fraction of $H_2O$ present in the gas
$\alpha$	surrounding absorptivity (=1.0)
$\epsilon$	particle emissivity (=0.8)
$\lambda$	particle burning rate, cm/sec
$\rho$	density, g/cm³
$\sigma$	Stefan-Boltzmann constant, cal/cm² sec°K⁴

### 2.3 Mohan's Model

C	average molecular velocity normal to the surface (cm/sec)
$C_t$	heat capacity of $B_2O_3(L)$ (cal/gm°K)
D	diffusion coefficient ( $cm^2/sec$ )
d	diameter of particle (cm)
h	thickness (cm)
k	effective distribution coefficient related to the ratio of the mole fraction of $O_2$ absorbed in $B_2O_3(l)$ to gas phase mole fraction
$k'$	distribution ratio (liquid phase to gas phase $O_2$ concentration)
L	sum of heat losses by radiation and conduction $\frac{cal}{cm^2 sec}$
P	total ambient pressure (atm)
$q_B$	heat liberated per unit mass of boron consumed at B (cal/g)
$q_C$	heat absorbed per unit mass of $B_2O_3$ vaporized at C (cal/g)
$R_B$ or C	regression rate of the surface (cm/sec)
$R^\circ$	universal gas constant ( $8.316 \cdot 10^{-7}$ erg/gm-mole °K)
T	temperature (°K)
t	time (sec)
$w_i$	atomic weight
X	mole fraction of $O_2$ in the ambient atmosphere
$x_a$	ratio equilibrium vapor pressure of $B_2O_3$ at $T_c$ to total pressure

$\alpha$	evaporation coefficient
$\epsilon$	emissivity
$\lambda$	gas phase thermal conductivity (cal/cm·sec °K)
$\rho_{B,C}$	density boron and $B_2O_2$ ( $gm/cm^3$ )
$\tau$	time for the new combustion regime to appear (sec)
$B,C$	surfaces

#### 2.4 Vovchuk's Model

$C_p$	molar specific heat
$D$	diffusion coefficient
$d_{do}$	initial diameter of the boron droplet
$H_i$	total enthalpy of species i
$\Delta H_i$	heat of reaction of species i
$I_i$	molar flux of species i
$M_B$	mass flow of the boron reacting in unit time
$P$	total pressure
$P_i$	partial pressure of species i
$Q_R^K$	radiative heat flux
$R$	universal gas constant
$r$	radius
$T$	temperature
$\epsilon$	emissivity
$\lambda$	thermal conductivity of gas
$\mu_i$	molecular weight
$v_i$	stoichiometric coefficients
$\rho_i$	density
$\sigma$	Stefan's constant
$\tau_r$	droplet combustion time

#### Subscripts

$B$	(molten) boron
$K$	particle or particle surface
$\infty$	infinity

Note: units not stated, therefore any consistent set of units may be used..

## 2.5 Edelman's Model

A	number of moles of oxygen per mole of product
a	the total (dimensionless) particle consumption rate
B	number of moles of boron per mole of product
$C_D$	drag coefficient
$C_p$	specific heat of the gas ( $\text{ft}^2/\text{sec}^2 \text{ }^\circ\text{K}$ )
$C_{p,s}$	specific heat of boron at the surface ( $\text{ft}^2/\text{sec}^2 \text{ }^\circ\text{K}$ )
$\Delta H_R$	heat of reaction (calorie/gram)
$K_S$	surface reaction rate constant
L	latent heat of vaporization
$M_B$	molecular weight of boron (g/g-mole)
$M_{N_2}$	molecular weight of nitrogen (g/g-mole)
$M_{O_2}$	molecular weight of oxygen (g/g-mole)
$M_{prod}$	molecular weight of the product (g/g-mole)
$M_s$	average molecular weight at the particle surface (g/g-mole)
P	pressure (in atmospheres)
$P_{V,B(T_p)}$	vapor pressure of boron (atm)
R	particle radius (feet)
$T_g$	gas temperature ( $^\circ\text{K}$ )
$T_p$	particle temperature ( $^\circ\text{K}$ )
$T_w$	temperature of the wall ( $^\circ\text{K}$ )
$V_g$	gas velocity (ft/sec)
$V_p$	particle velocity (ft/sec)
$Y_{B,S}$	mass fraction of boron at the surface of the particle
$Y_{N_2,S}$	mass fraction of nitrogen at the surface
$Y_{O_2,S}$	mass fraction of oxygen at the surface of the particle
$Y_{O_2,\infty}$	mass fraction of oxygen in the surrounding (gas)
$Y_{prod,S}$	mass fraction of the product at the particle surface
$\alpha$	fraction of vaporized product
$\delta_s$	particle bulk density (slugs/ $\text{ft}^3$ )
$\epsilon$	emissivity
$\lambda$	the thermal conductivity of nitrogen (lbs force/sec $^\circ\text{K}$ )
$\rho_g$	gas density (slugs/ $\text{ft}^3$ )

$\rho_s$   
 $\sigma$

density at the surface of the particle (slugs/ft<sup>3</sup>)  
Stefan Boltzmann constant (lbs force/ft·sec °K<sup>4</sup>)

was to develop a code which could stand alone as a tool to be used in the investigation of single-particle combustion phenomena, but which could also be easily incorporated into the modular model format without substantial modification. This dual capability was achieved by structuring the code as a series of subroutines which do not depend on the basic code in which they are found. In the stand-alone code they are called out of a main routine which does little more than obtain the needed inputs and call the first of them; in the modular approach this calling subprogram is a simple routine which corrects existing data to the units and variables required and calls the boron particle subroutine package. The subroutine package itself needs no modification in either case.

Both models involve the solution of a set of coupled ordinary differential equations. The integration was carried out using subroutine HPCG, one of the standard differential equation solvers. HPCG uses Hamming's modified predictor-corrector method to obtain an approximate solution to the system. Although not self-starting (the initial solution is obtained using a Runge-Kutta technique) the technique is superior to the Runge-Kutta in that it requires evaluation of the right-hand side only twice per step. Furthermore, because the local truncation error falls out automatically calculation of the proper step size is facilitated (it has the capability of moving in either direction as the solution proceeds, but it never exceeds an input maximum). The technique used is a stable fourth order scheme.

### 3.2.1 King's Model

#### 3.2.1.1 Model Description

King's model includes the inhibiting effect of the boric oxide layer on ignition and explicitly calculates the particle melt time before ignition. It is thus the better model of the ignition process. However, because it does not include the kinetically controlled terms, it is poor for predicting results for ignited particles (indeed, it predicts a total thermal runaway).

The basic model consists of four coupled equations relating particle temperature, particle size, oxide layer thickness and the fraction of the particle which is melted. It can be expressed as follows:

$$\frac{dT_p}{dt} = \begin{cases} \frac{R_B Q_{RX} - R_E \Delta H_{vap} - R_H \Delta H_H + 4\pi(r_p+x)^2 [h(T_\infty - T_p) + \sigma \epsilon \alpha_R (T_{rad}^4 - T_p^4)]}{\frac{4}{3} \pi r_p^3 \rho_B C_{p_{BS}} + 4\pi r_p^2 x \rho_{B_2O_3} C_{p_{B_2O_3}}}, & T_p < 2450, f=0 \\ 0, & T_p = 2450, f<1 \\ \frac{R_B Q_{RX_2} - R_E \Delta H_{vap} - R_H \Delta H_H + 4\pi(r_p+x)^2 [h(T_\infty - T_p) + \sigma \epsilon \alpha_R (T_{rad}^4 - T_p^4)]}{\frac{4}{3} \pi r_p^3 \rho_B C_{p_{BL}} + 4\pi r_p^2 x \rho_{B_2O_3} C_{p_{B_2O_3}}}, & T_p > 2450, f=1 \end{cases} \quad (3)$$

where

$C_{p_{B_2O_3}}$	liquid boric oxide heat capacity (cal/gm °K)
$C_{p_{BL}}$	liquid boron heat capacity (cal/gm °K)
$C_{p_{BS}}$	solid boron heat capacity (cal/gm °K)
$h$	gas-particle heat transfer coefficient (cal/gm °K)
$Q_{RX}$	heat release of $B(S) + \frac{3}{4} O_2 \rightarrow \frac{1}{2} B_2O_3(\ell)$ (cal/gm-mole)
$Q_{RXZ}$	heat release of $B(L) + \frac{3}{4} O_2 \rightarrow \frac{1}{2} B_2O_3(\ell)$ (cal/gm-mole)
$R_B$	molar rate of boron consumption (gm-mole/sec)
$R_H$	molar rate of removal of $B_2O_3$ by water reaction (gm-mole/sec)
$r_p$	particle radius (cm)
$T_p$	particle temperature (°K)
$T_{rad}$	surroundings radiation temperature (°K)
$T_\infty$	free stream gas temperature (°K)
$x$	oxide layer thickness (cm)
$\alpha_R$	surroundings absorptivity
$\Delta H_H$	heat absorbed by the reaction of $H_2O$ with $B_2O_3(\ell)$ (cal/gm-mole)

$\Delta H_{vap}$	heat of vaporization of $B_2O_3(l)$ (cal/gm-mole)
$\epsilon$	particle emissivity
$\rho_B$	boron density ( $gm/cm^3$ )
$\rho_{B_2O_3}$	boric oxide density ( $gm/cm^3$ )
$\sigma$	Stefan-Boltzman Constant ( $cal/cm^2 sec^{-1} K^4$ )

$$\frac{df}{dt} = \begin{cases} 0, T_p < 2450, f=0 \\ \frac{R_B Q_{RX} - R_E \Delta H_{vap} - R_H \Delta H_m + 4\pi(r_p+x)^2 [h(T_\infty - T_p) + \sigma \epsilon \alpha_R (T_{rad}^4 - T_p^4)]}{4/3 \pi r_p^3 \rho_B \Delta H_m}, T_p = 2450, f<1 \\ 0, T_p > 2450, f=1 \end{cases} \quad (4)$$

where  $\Delta H_m$  = heat of fusion of boron (cal/gm), and the other variables are as defined above.

$$\frac{dr_p}{dt} = - \frac{R_B (\text{MW})_B}{4\pi r_p^2 C_B} \quad (5)$$

where  $(\text{MW})_B$  = boron atomic weight (gm/gm-mole), and the other parameters are as above. Finally,

$$\frac{dx}{dt} = \frac{(R_B/2 - R_E - R_H)(\text{MW})_{B_2O_3}}{4\pi r_p^2 C_{B_2O_3}} \quad (6)$$

where  $(\text{MW})_{B_2O_3}$  is the boric oxide molecular weight (gm/gm-mole) and all other variables are already defined.

As can be seen, the King model is actually three models, of which one is selected based on current particle temperature, and melt history. This requires careful handling in the coding. The HPCG routine needs a subroutine to evaluate the derivatives at each time step. One cannot, however, merely wait until the particle temperature meets some criterion, then start using the

melt equation because the integrator may call this routine many times for every final solution it accepts. Furthermore, there is no easy way to tell while in the derivative routine whether or not the solution this time will be accepted. Thus it was necessary to write three essentially separate routines for the three states of the particle heating, melt, and burn.

Initially the time range of interest is passed to the integrator, which starts with the assumption that the particle is not melted. When (and if) the particle reaches (or passes) the melt temperature ( $2450^{\circ}\text{K}$ ) the integration is stopped, values are set back to those at which  $T_p = 2450$  exactly, and the integration procedure is initialized for the new problem (defined now as the calculation of the fraction of the boron which is liquid,  $f$  (Eq. 4)). When the liquid fraction reaches (or passes) unity, the integration is again stopped and the values are again reset (this time to those at which the liquid fraction is exactly 1.0) and the integration is initialized for the burn problem. This methodology allows automatic correct handling of those cases in which the particle never melts, those in which only partial melting occurs, as well as those cases in which ignition occurs. The implementation is all automatic and transparent to the user.

Because the individual time steps are small with respect to the variables being calculated it was decided that a linear interpolation gave sufficient accuracy, and represented the best approach to the problem of resetting the variables at the boundaries of the particle states. A comparison of King's results with those obtained using the SAI code verifies the adequacy of this approach.

The approach was checked by recalculating some of King's original results using the King model code. Two cases were selected for this on the basis of near-critical temperature determining whether or not ignition occurred. In both cases the particle radius is 10 microns and the oxide layer is 0.1 microns. The initial particle temperature is  $1800^{\circ}\text{K}$ ; the oxygen mole fraction is 0.2 and the pressure is 5 atmospheres.

The first case has a gas temperature of  $2100^{\circ}\text{K}$ . Fig. 9 shows the particle temperature histories as calculated by King and by SAI. The results are essentially identical. The observed differences are more likely due to inaccuracies in reading the King curve from Ref. 16 than to be actual numerical

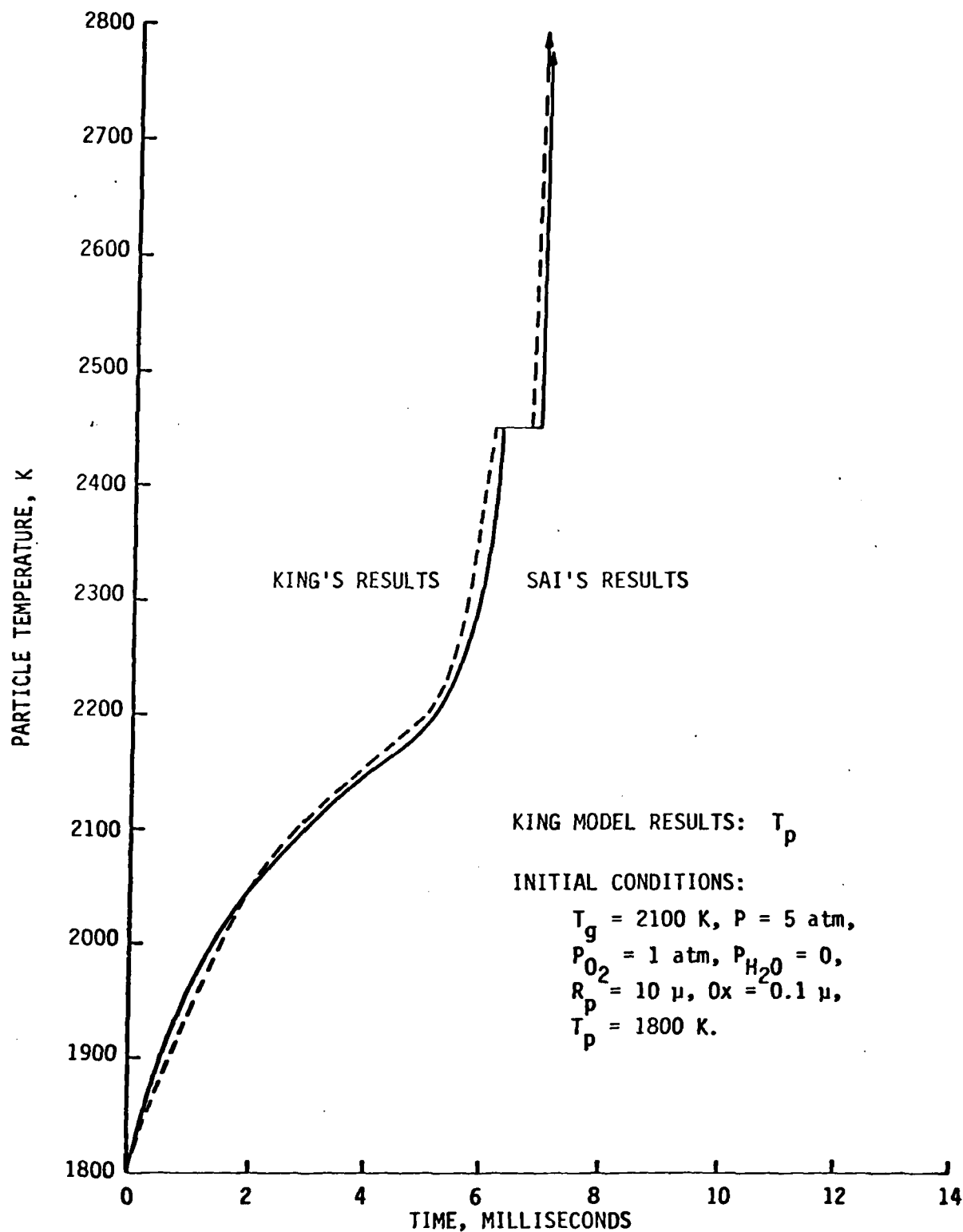


FIGURE 9. Temperature history for the  $2100^\circ$  case.

differences. Fig. 10 compares the two calculations of the oxide layer thickness as a function of time. Again it is seen that the two calculations are essentially identical. Fig. 11 gives the particle radius history for the SAI calculation (King did not present this result).

The second comparison case was run for an identical case except that the gas temperature was 2000°K. Here King shows that true ignition does not occur. Fig. 12 shows that the SAI code predicts essentially the same result as was obtained by King. Fig. 13 also confirms this result for the oxide layer thickness (the apparent difference again may well be due to difficulty in reading the detail on the plot of King's results - if the data were plotted in the same scale as they appear in Ref. 16 there would be no discernable difference). Comparison of Figs. 11 and 14 shows very little difference initially. However, in the degenerate combustion case the initial trend is continued whereas in the full ignition case (Fig. 11) the effect of particle heatup and melting is evident.

The two cases taken together demonstrate that the King model has been faithfully reproduced in the SAI code. The system behaves just as predicted by King on both sides of the critical gas temperatures.

### 3.2.2 Edelman's Model

Edelman's model (Refs. 20, 21) neglects the inhibiting effect of the boric oxide layer on ignition and fails to calculate the particle melt time. However, it includes all the kinetically controlled mechanisms in the combustion equations. Consequently, it is superior to King's model for examination of what happens after the particle has ignited.

The full Edelman model consists of nine coupled ordinary differential equations. However, as expanded by Edelman (Ref. 21) the system can be simplified to three equations without significant loss of accuracy; the remaining equations, although actually functions of time, can be treated algebraically. It is the simplified version which is here presented. The three differential equations are:

$$\frac{dv_p}{dt} = \frac{3C_D p(v_g - v_p)^2}{8R\delta_s}, \quad (7)$$

KING MODEL RESULTS: O<sub>x</sub>

INITIAL CONDITIONS:

$T_g = 2100 \text{ K}$ ,  $P = 5 \text{ atm}$ ,

$P_{O_2} = 1 \text{ atm}$ ,  $P_{H_2O} = 0$ ,

$R_p = 10 \mu$ ,  $O_x = 0.1 \mu$ ,

$T_p = 1800 \text{ K}$

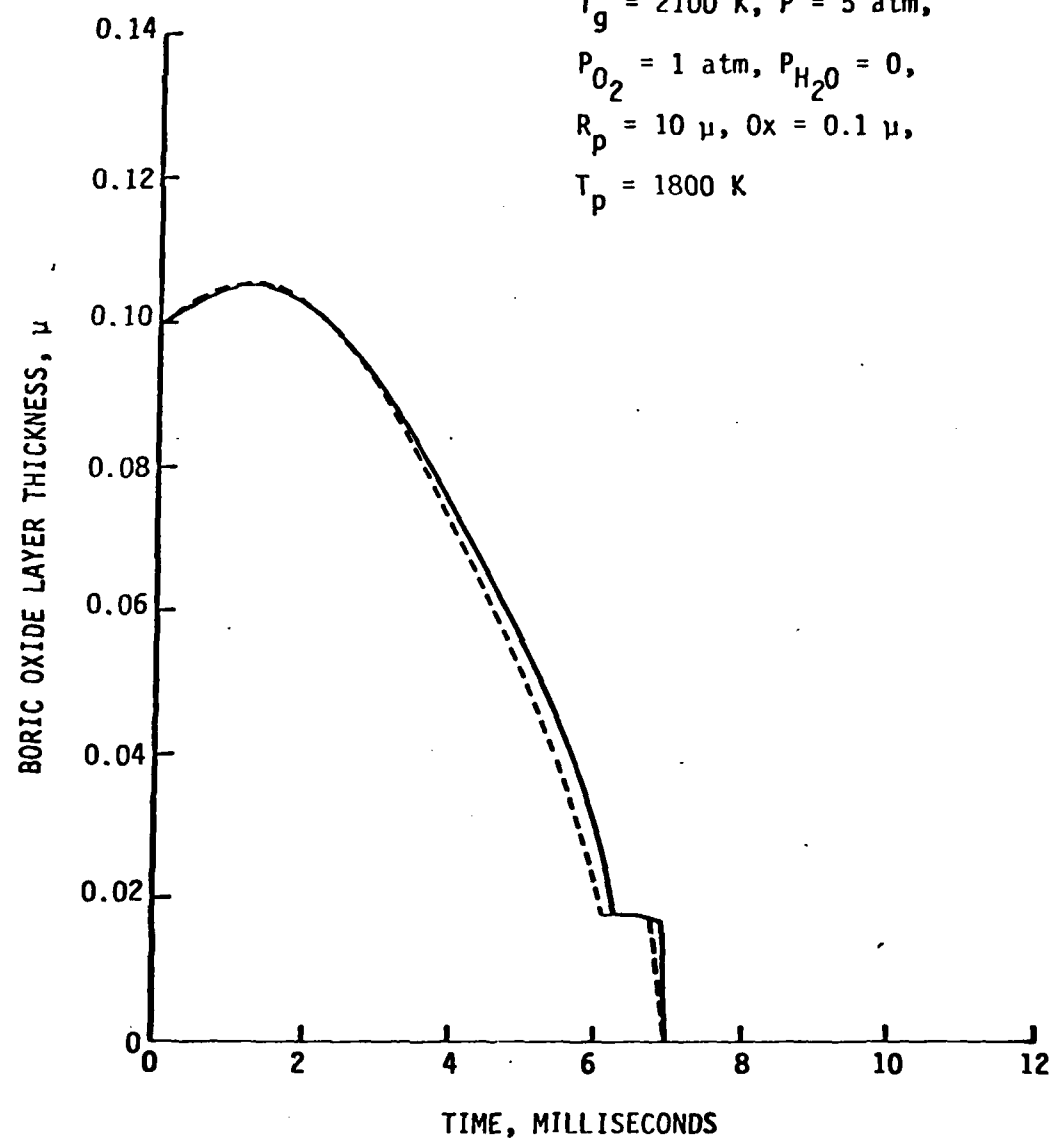


FIGURE 10. Oxide layer history for the 2100° case.

KING MODEL RESULTS:  $R_p$

INITIAL CONDITIONS:

$T_g = 2100 \text{ K}$ ,  $P = 5 \text{ atm}$ ,

$P_{O_2} = 1 \text{ atm}$ ,  $P_{H_2O} = 0$ ,

$R_p = 10 \mu$ ,  $O_x = 0.1 \mu$ ,

$T_p = 1800 \text{ K}$

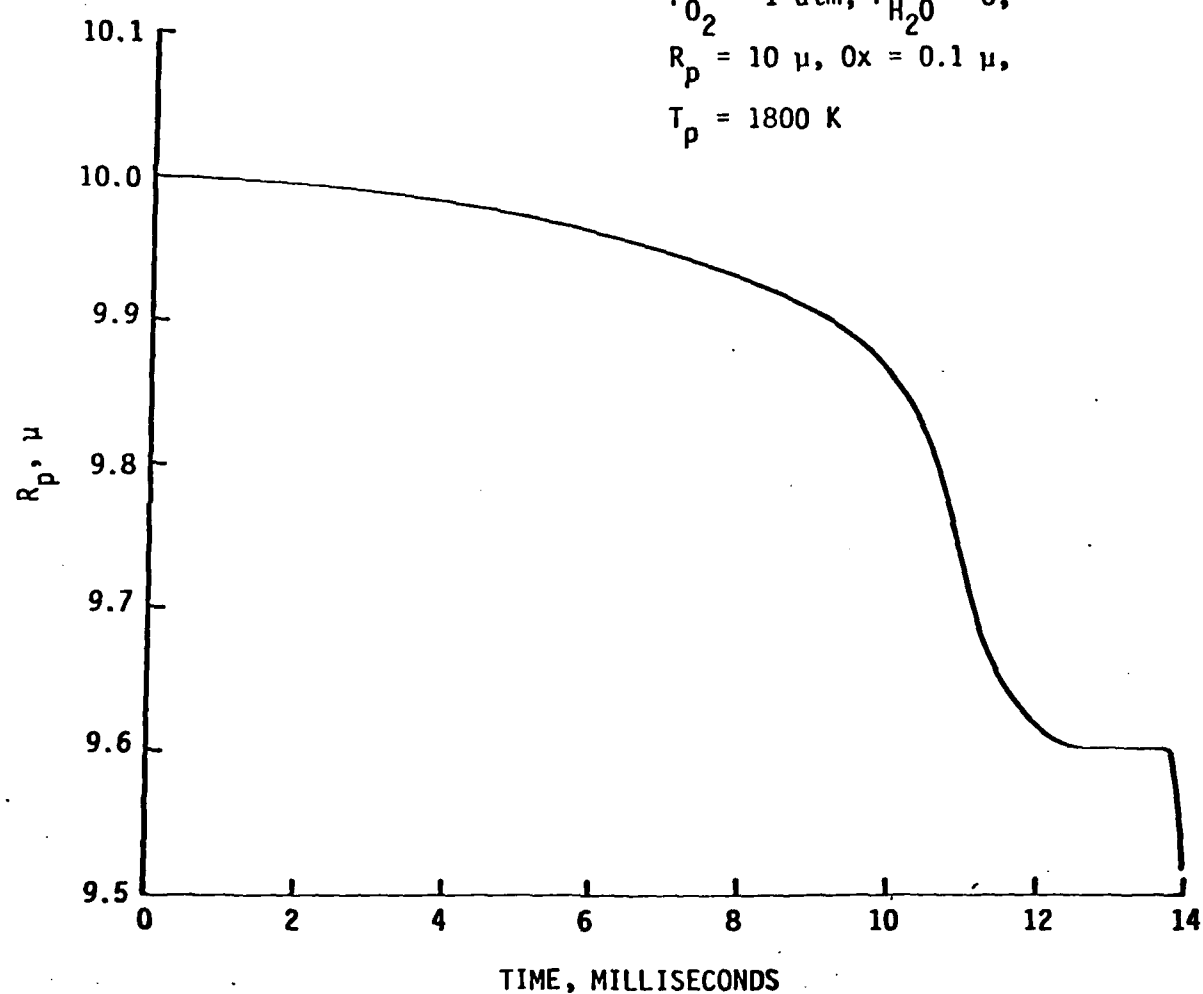


FIGURE 11. Particle radius history in the  $2100^\circ$  case.

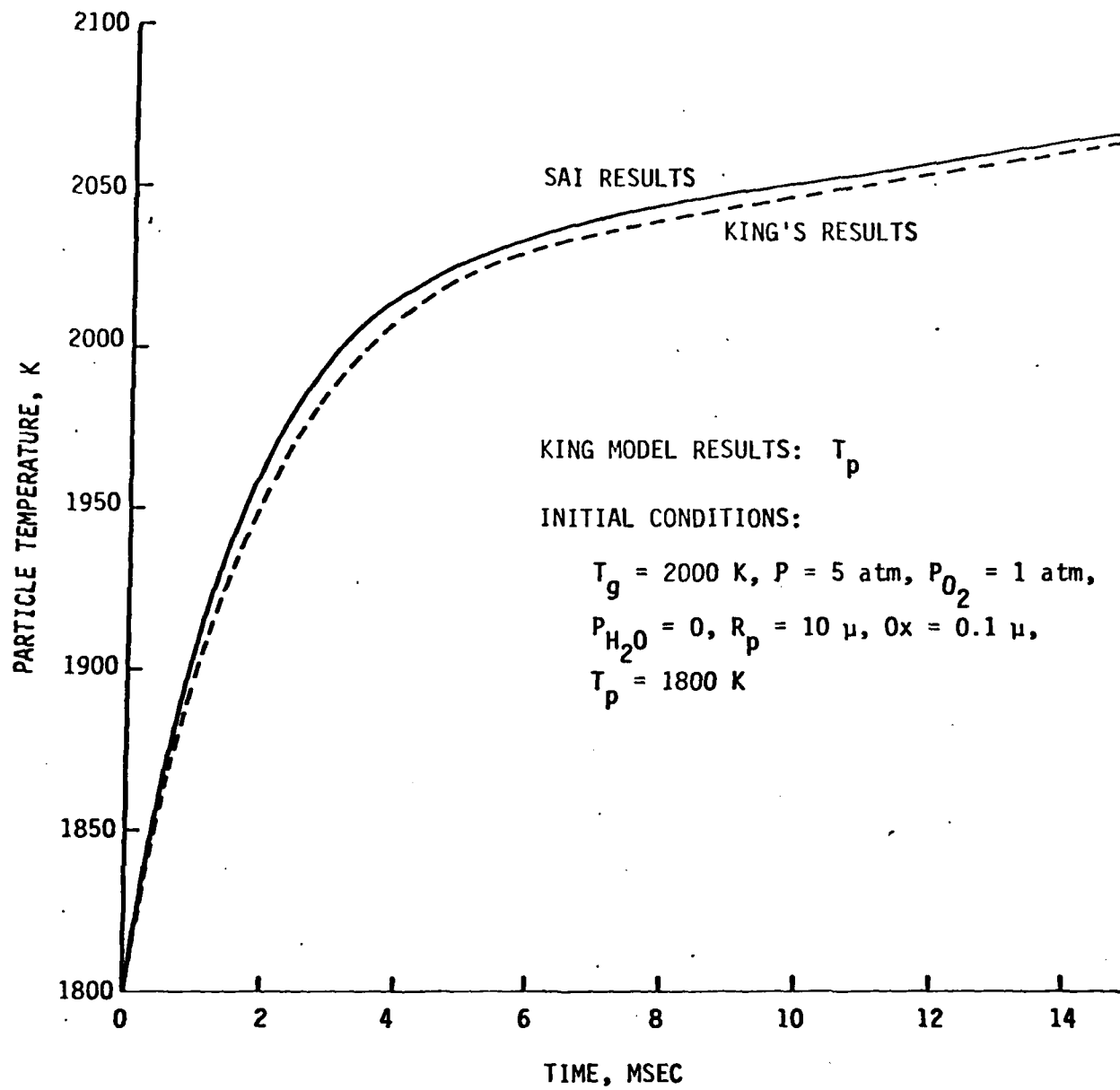


FIGURE 12. Particle temperature history in the 2000° case.

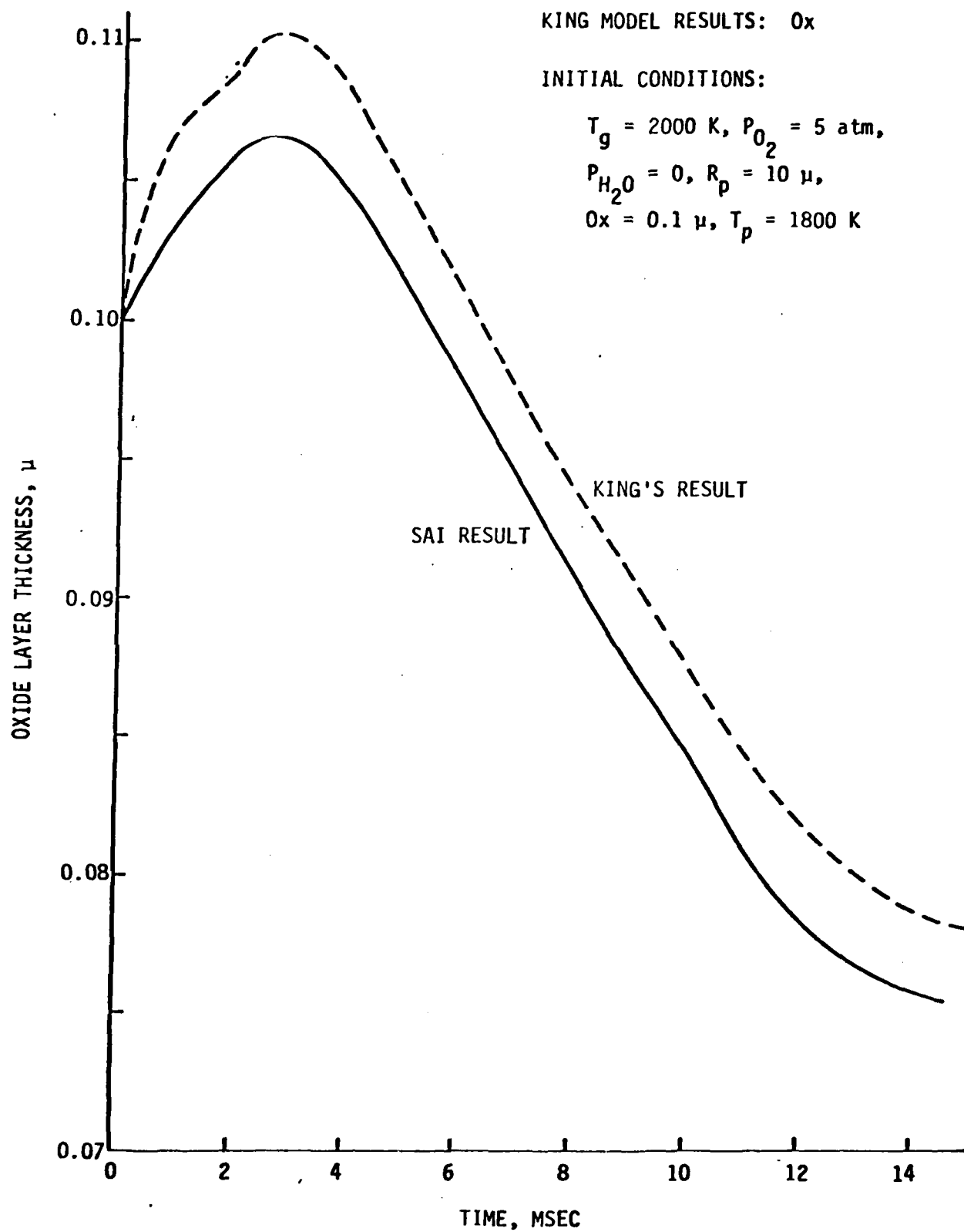


FIGURE 13. Oxide layer thickness history for the 2000° case.

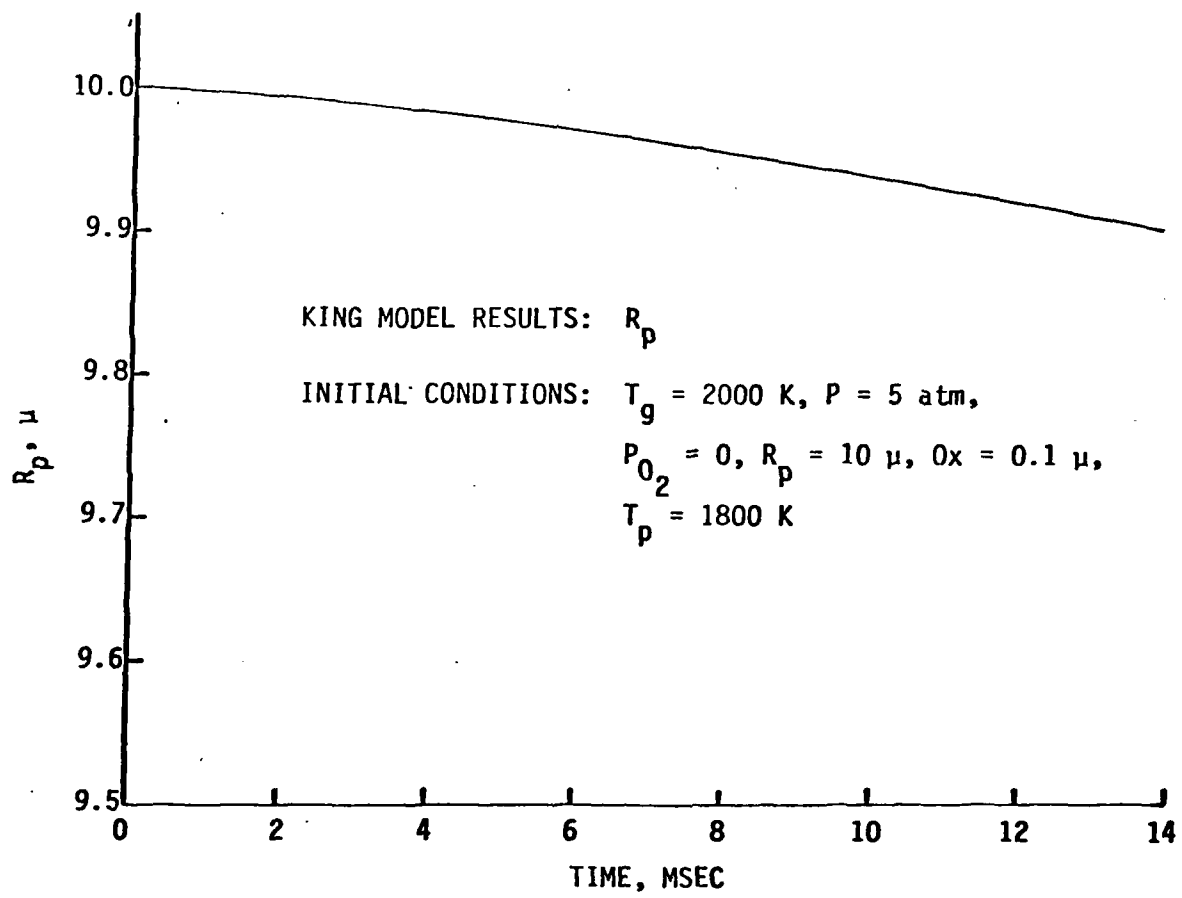


FIGURE 14. Particle radius history in the 2000° case.

where  $C_D$  = drag coefficient  
 $\rho_g$  = gas density (slugs per cubic foot)  
 $V_g$  = gas velocity (ft/sec)  
 $V_p$  = particle velocity (ft/sec)  
 $R$  = particle radius (feet)  
and  $\delta_s$  = particle bulk density (slugs/ft<sup>3</sup>)

$$\frac{dR}{dt} = \frac{-a\lambda N_u}{2R\delta_s C_p}, \quad (8)$$

where  $a$  = the total (dimensionless) particle consumption rate (see Eq. 10)  
 $\lambda$  = the thermal conductivity of nitrogen (in pounds force/sec °K)  
 $Nu$  = Nusselt number  
 $C_p$  = specific heat of the gas (in ft<sup>2</sup>/sec<sup>2</sup> °K), and the remaining variables as already defined.

$$\frac{dT_p}{dt} = \frac{3a\lambda Nu}{2\delta_3 C_p R^2 C_p} \left[ \frac{C_p(T_g - T_p)}{e^a - 1} - L + \frac{AK_s(2C_p \rho_s R) Y_{O_2,s} M_B \Delta H_R}{a\lambda Nu M_{O_2}} - \frac{2\sigma \epsilon R C_p (T_p^4 - T_w^4)}{a\lambda Nu} \right] \quad (9)$$

where  $C_{p_s}$  = specific heat of boron at the surface (ft<sup>2</sup>/sec<sup>2</sup> °K)  
 $T_g$  = gas temperature (°K)  
 $T_p$  = particle temperature (°K)  
 $L$  = latent heat of vaporization  
 $A$  = number of moles of oxygen per mole of product  
 $K_s$  = surface reaction rate constant  
 $\rho_s$  = density at the surface of the particle (slugs/ft<sup>3</sup>)  
 $Y_{O_2,s}$  = mass fraction of oxygen at the surface of the particle  
 $M_B$  = molecular weight of boron (g/g.mole)  
 $\Delta H_R$  = heat of reaction (calorie/gram)  
 $M_{O_2}$  = molecular weight of oxygen (g/g.mole)

$\sigma$  = Stefan-Boltzmann Constant (lb-force/ft<sup>2</sup>·sec °K<sup>4</sup>)

$\epsilon$  = emissivity

$T_w$  = temperature of the wall (°K)

and other parameters are as defined above.

The values for the remainder of the time-varying parameters are treated as simple algebraic equations (using the current value of  $T_p$  and R) as follows

$$a = \frac{88.662C_p\alpha R}{\lambda Nu} \sqrt{\frac{M_B}{T_p}} \left[ P_{V,B}(T_p) - \frac{M_s}{M_B} Y_{B,S} P \right] + \frac{2M_B K_s Y_{O_2,s} C_p \rho_s R A}{M_{O_2} \lambda Nu} \quad (10)$$

where  $\alpha$  = fraction of vaporized product

$P_{V,B}(T_p)$  = vapor pressure of boron (atm)

$M_s$  = average molecular weight at the particle surface (g/g·mole)

$Y_{B,S}$  = mass fraction of boron at the surface of the particle

$P$  = pressure (in atmospheres)

and other variables are as previously defined.

$$Y_{O_2,s} = \frac{Y_{O_2,\infty} e^{-a}}{1 + BK_s \left[ \frac{2(1-e^{-a})C_p \rho_s R}{a \lambda Nu} \right]} \quad (11)$$

where  $Y_{O_2,\infty}$  = mass fraction of oxygen in the surrounding (gas)

$B$  = number of moles of boron per mole of product

and the remaining variables are as previously defined.

$$Y_{B,S} = (1-e^{-a}) \left[ 1 - AK_s \frac{2Y_{O_2,s} C_p \rho_s R}{a \lambda Nu} \left( \frac{M_B}{M_{O_2}} \right) \right] \quad (12)$$

$$Y_{prod,s} = (1-e^{-a}) \left[ \frac{2K_s Y_{O_2,s} C_p \rho_s R}{a \lambda Nu} \left( \frac{M_{prod}}{M_{O_2}} \right) \right] \quad (13)$$

where  $\gamma_{prod,s}$  = mass fraction of the product at the particle surface  
 $M_{prod}$  = molecular weight of the product g/g.mole)

and the remaining parameters are defined above

$$M_s = \text{average molecular weight at the surface} = \left[ \frac{\gamma_{O_2,s}}{M_{O_2}} + \frac{\gamma_{B,s}}{M_B} + \frac{\gamma_{prod,s}}{M_{prod}} + \frac{\gamma_{N_2,s}}{M_{N_2}} \right]^{-1} \quad (14)$$

where  $M_{N_2}$  = molecular weight of nitrogen (g/g.mole)

$\gamma_{N_2,s}$  = mass fraction of nitrogen at the surface

and the remaining variables as previously defined.

$$\gamma_{N_2,s} = (1 - \gamma_{O_2,s} - \gamma_{B,s} - \gamma_{prod,s}) \quad (15)$$

The Edelman model is, in a sense, more easily implemented than King's because it does not treat separate realms of phenomena. However, as will be seen from an examination of Eqs. 10-13, virtually everything is a function of  $a$ , which itself is a function of both  $\gamma_{O_2,s}$  and  $\gamma_{B,s}$ . Hence one is faced with a set of three highly non-linear equations which are strongly coupled.

In the original work done by Edelman an iterative solution technique was implemented which depended on the ratio of surface mass fractions to surroundings mass fractions to converge to a solution. However, all attempts to implement this technique were met with uniform failure. Finally this approach was abandoned and a Newton-Raphson scheme was derived for the solution of the set of equations. This approach quickly led to convergence. However, a few troublesome anomalies appeared, the most serious of which was a calculated negative mass fraction for the product in some areas. Since this was extremely small (of order  $10^{-9}$ ) it was decided to be due to inherent inaccuracy in the numerics (and/or machine roundoff) and zeroed out when it occurred in a final converged result (but not before). Consequently, the final convergence criteria were: a change in all three variables from one step to another of less than  $10^{-7}$  or a change in all three variables of less than 0.1%. If either

of these criteria were met, the solution was considered to have converged unless a negative mass fraction occurred. A significant negative mass fraction causes the routine to iterate again. (A significant negative is defined to be greater in absolute value than  $10^{-8}$ ).

Initial results from the Edelman model suggest that the diffusion terms are not the dominant ones in the equations. Hence the results suggest that the driver mechanism is kinetics; indeed, Fig. 15 shows that the particle radius decline is very close to linear with time. Even the temperature curve for the 17.3 micron particle is reasonably close to linear (Fig. 16). Results for a larger particle (50 micron diameter) are also nearly linear (Fig. 17), and a plot of the square of particle diameter vs. time (Fig. 18) does show some curvature.

### 3.3 PARTICLE TRACKING FOR SLURRY FUEL COMBUSTION ANALYSES

The combined effects of continuous reaction of boron particles and the non-uniform velocity and temperature fields within the combustor provide conditions resulting in a spectrum of particle sizes at every point in the flow. To completely specify the particle reaction rate and the production of gas phase species, the local particle size and number density distribution must be known. This in turn requires the development of a methodology for tracking the particle history throughout the flow.

To track the particle history through the flow, the total amount of particulate material present at every point in the field is divided into a set of categories. These categories can be based on any parameter which can be used to differentiate particles: for the boron application both particle size and the thickness of the liquid  $B_2O_3$  layer ( $X$ ) on the particle surface are relevant parameters. Both parameters may be used, with liquid layer thickness forming a subclassification in a basic particle size classification, but it should be kept in mind that each category used introduces a new variable in the overall combustor model with associated transport equation and storage requirements.

For simplicity, consider a categorization based on particle size. Within each size range, all particles are combined to form an average with a volume

INITIAL CONDITIONS:  $T_g = 2460$  K,  $P = 1$  atm,  
 $\alpha_{O_2} = 0.4$ ,  $R_p = 17.3$ ,  
 $T_p = 300$  K

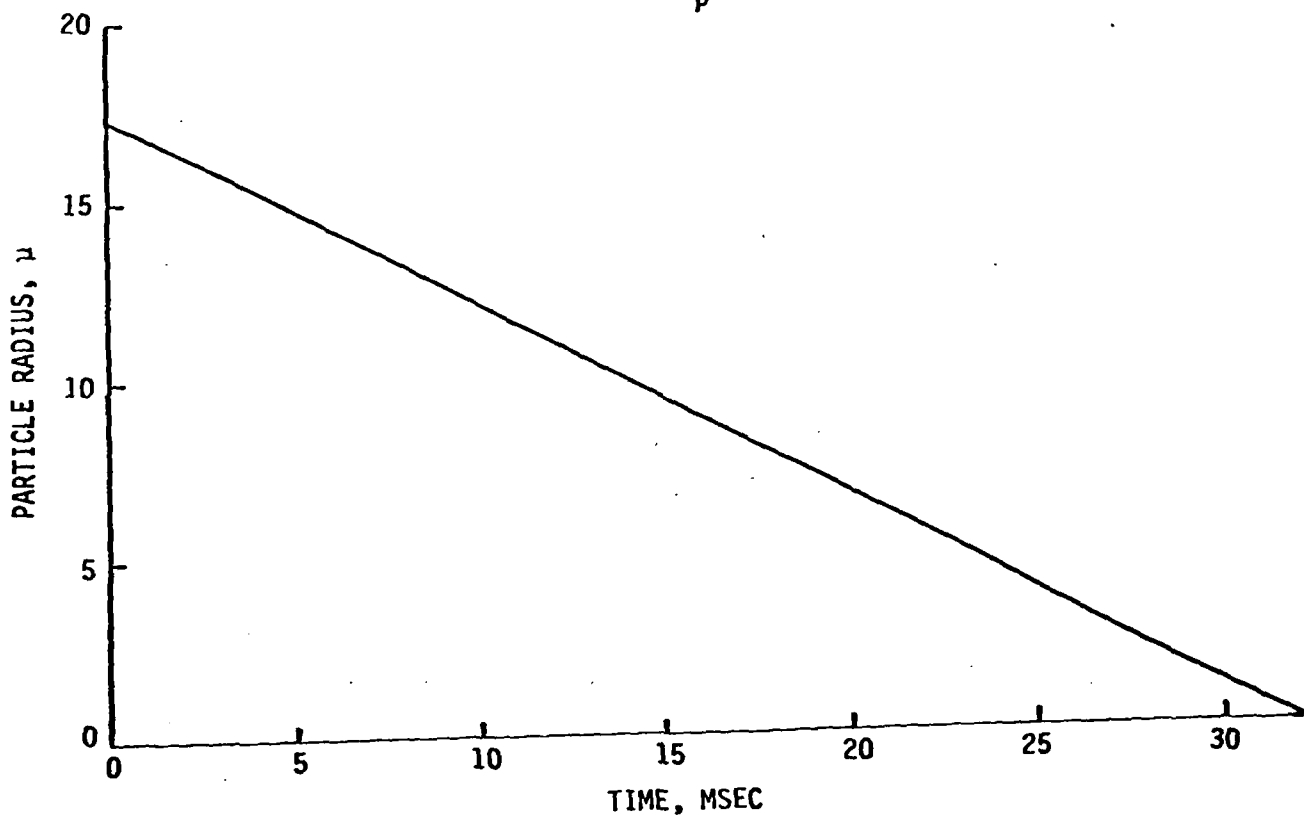


FIGURE 15. Particle radius history for the  $17.3 \mu$  particle.

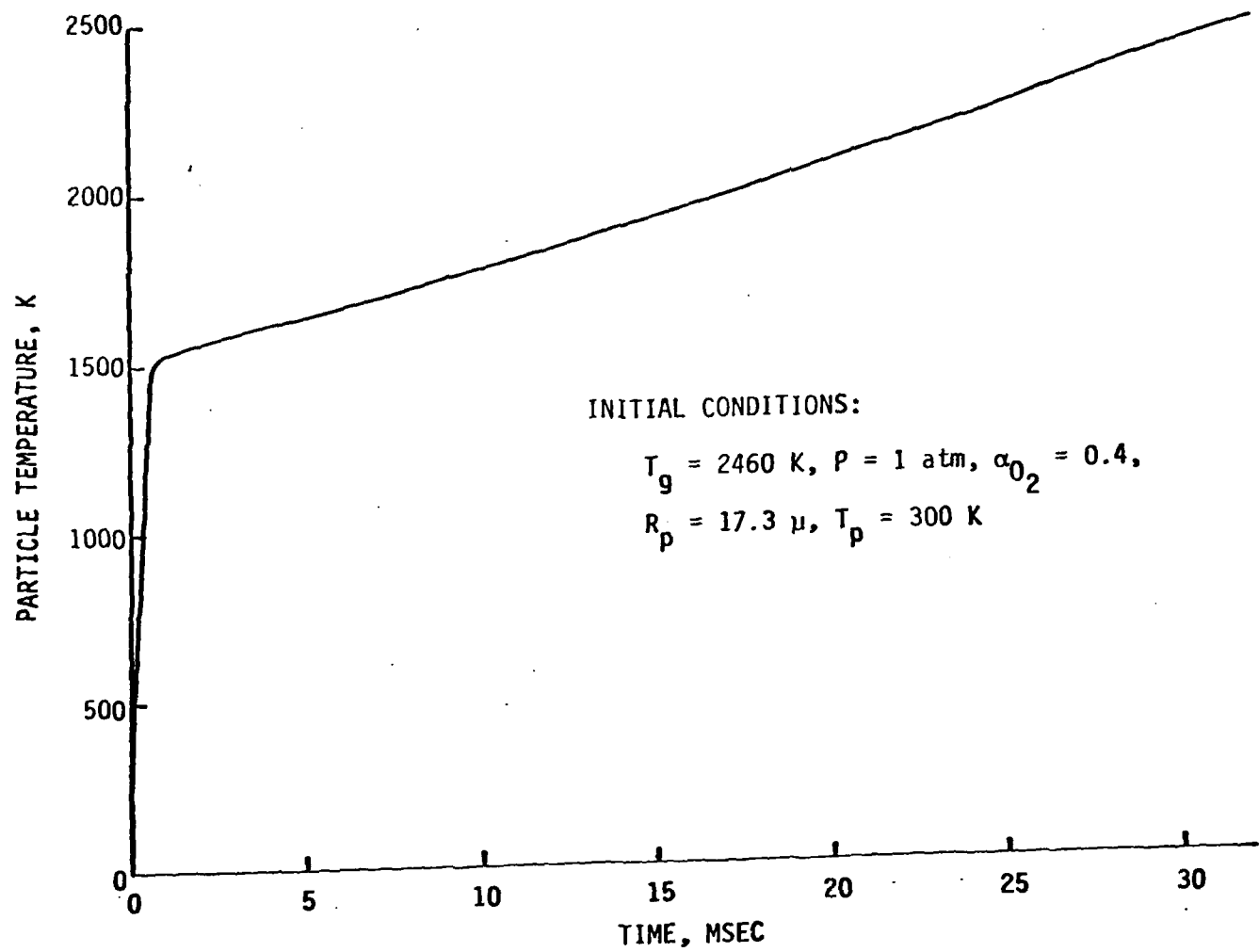


FIGURE 16. Particle temperature history for the  $17.3 \mu$  particle.

INITIAL CONDITIONS:  $T_g = 2460$  K,  $P = 1$  atm,  
 $\alpha_{0_2} = 0.4$ ,  $R_p = 25 \mu$ ,  $T_p = 300$  K

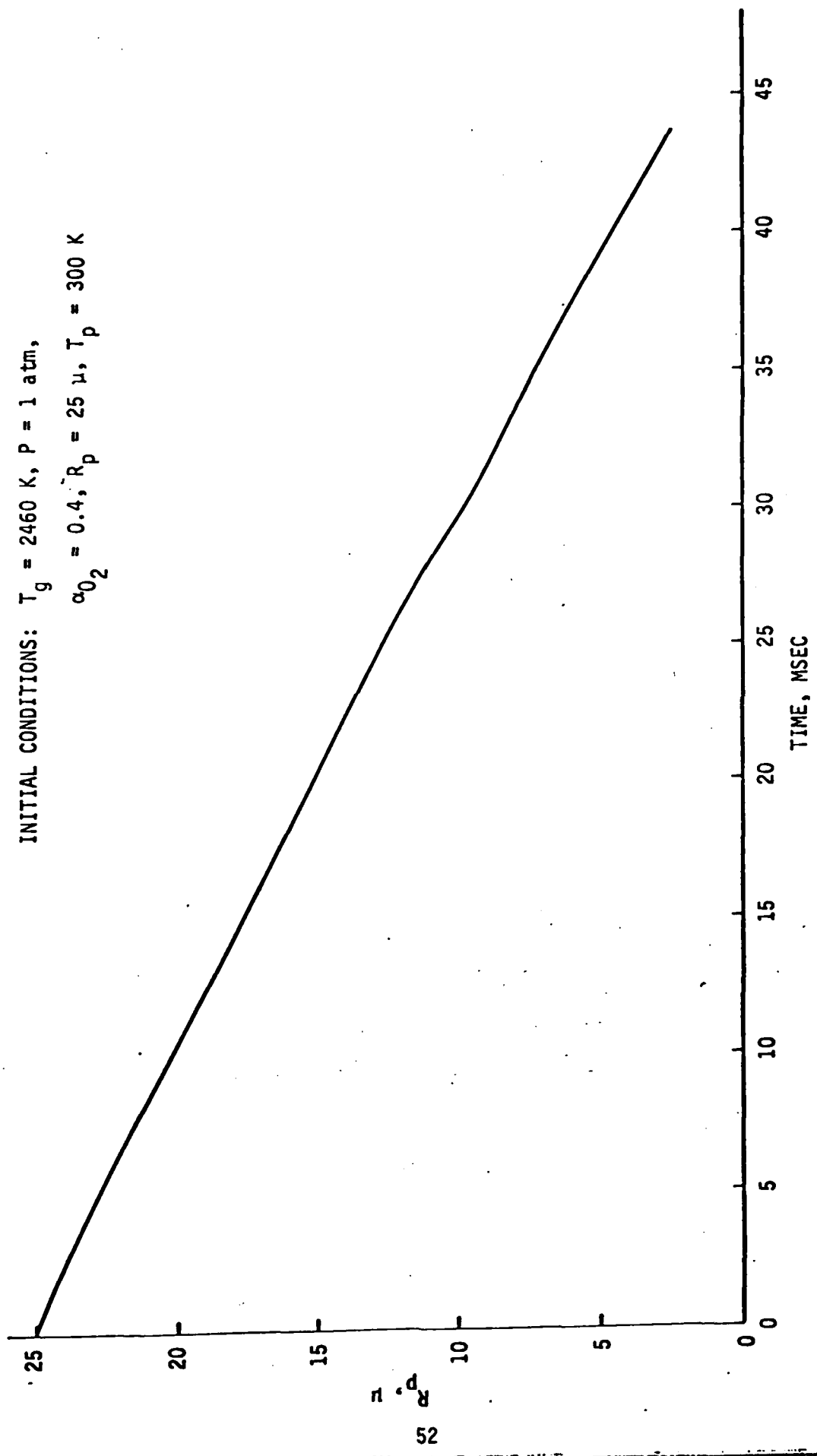


FIGURE 17. Particle radius history for the  $25 \mu$  particle.

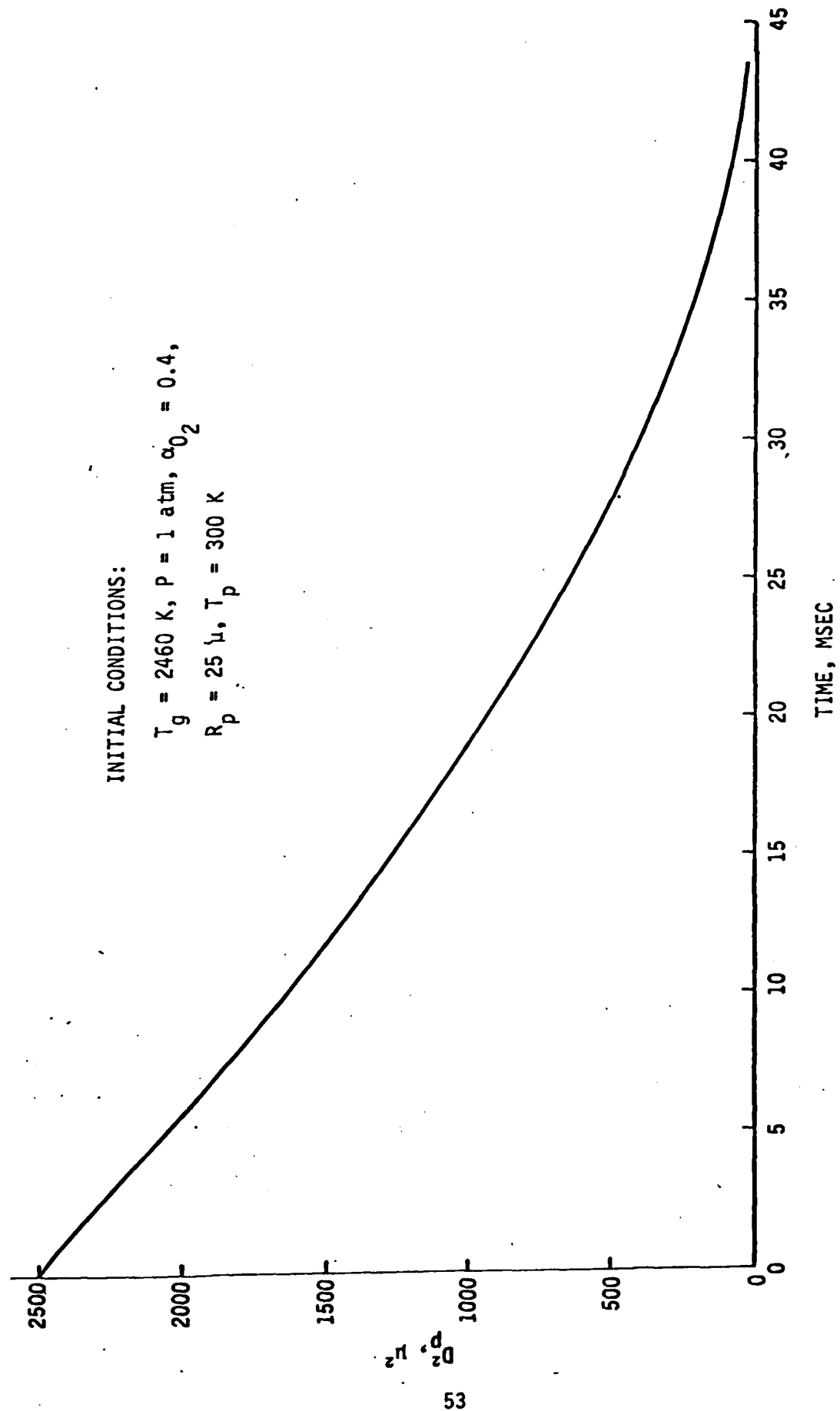


FIGURE 18. Square of particle diameter as a function of time.

to surface area ratio equal to that of the summation over all contributions. This equivalent particle size is the Sauter mean value and is expressed as

$$r_s = \sum n_i r_i^3 / \sum n_i r_i^2 \quad (16)$$

where  $n_i$  particles have radius  $r_i$ . The mass fraction of each category is equal to the sum of the mass fractions of each contribution. With the average size of category particles and the total category mass fraction known, the appropriate number of equivalent particles is established for every class. This representation provides an exact equivalence for the subsequent rate process provided the rate of change of mass depends directly upon the particle surface area.

The particle distribution array in terms of size, mass fraction, and number in each category at every grid point can only be altered by changes in size of the particle due to chemical reaction (which can also, for boron, involve changes in liquid layer thickness) and by diffusion of particles from the neighboring flow. The radius of the particle changes in accordance with the particle consumption expression as the flowfield develops. Thus, after every step, the new particle size is given by

$$r = r_0 + \int_{x_0}^x \frac{dr}{dx} \Delta x \quad (17)$$

Where the step size,  $\Delta x$ , is evaluated based on the stability criteria incorporated in the modular model. After every step the updated radius array must be reclassified in order to account for the transition of particles from one category to another. Since it is possible for more than one contribution to be made to a particular category, the total category mass must then be reaveraged using the Sauter criteria, to establish the proper radius and number for the group. The particle array in terms of mass fraction, size and number density resulting from the kinetics of the combustion process will be defined as:

$$\begin{aligned} G(J,I)_k \\ R(J,I)_k & \text{ at grid point } \binom{n+1}{m} \\ N(J,I)_k \end{aligned}$$

Each category in the particle array is altered by the diffusion of particles of the same category from neighboring upstream locations. Subdividing the particle mass fraction  $\alpha_i$  into each separate category and treating the category mass fractions as separate species, the diffusion equation can be written in finite difference form in von Mises coordinates as

$$\alpha_{i,n+1,m} = \alpha_{i,n,m} + \Delta x \left( \frac{W_i}{u} \right)_{n,m} + \frac{\Delta x}{\psi (\Delta \psi)^2} \left\{ \left( \frac{b}{Sc} \right)_{n,m+\frac{1}{2}} \alpha_{i,n,m+1} - \left[ \left( \frac{b}{Sc} \right)_{n,m+\frac{1}{2}} + \left( \frac{b}{Sc} \right)_{n,m-\frac{1}{2}} \right] \alpha_{i,n,m} + \left( \frac{b}{Sc} \right)_{n,m-\frac{1}{2}} \alpha_{i,n,m-1} \right\} \quad (18)$$

where the  $n,m$  subscripts refer to the grid point locations shown in Fig. 19.

The second term in Eq. 18 represents the change in  $\alpha_i$  due to the kinetics process as the flow moves downstream from  $n$  to  $n+1$ . The sum of the first two terms is the total mass fraction of category particles present downstream due to kinetic processes, and the remaining term represents the contribution to the mass fraction from diffusion. Noting Fig. 19, the diffusional term can be split into the contributions from each of the three upstream points:

$$\Delta G_1 = \frac{\Delta x}{\psi (\Delta \psi)^2} \left( \frac{b}{Sc} \right)_{n,m+\frac{1}{2}} \alpha_{i,n,m+1} \quad (19)$$

$$\Delta G_2 = - \frac{\Delta x}{\psi (\Delta \psi)^2} \left[ \left( \frac{b}{Sc} \right)_{n,m+\frac{1}{2}} + \left( \frac{b}{Sc} \right)_{n,m-\frac{1}{2}} \right] \alpha_{i,n,m} \quad (20)$$

$$\Delta G_3 = \frac{\Delta x}{\psi (\Delta \psi)^2} \left( \frac{b}{Sc} \right)_{n,m-\frac{1}{2}} \alpha_{i,n,m-1} \quad (21)$$

For each of the categories present at a given grid point, we may express the category mass fraction as

$$G(J,I)n+1,m = \left[ \Delta x \left( \frac{W_i}{u} \right)_{n,m} \right] + \Delta G_1 + \Delta G_2 + \Delta G_3 \quad (22)$$

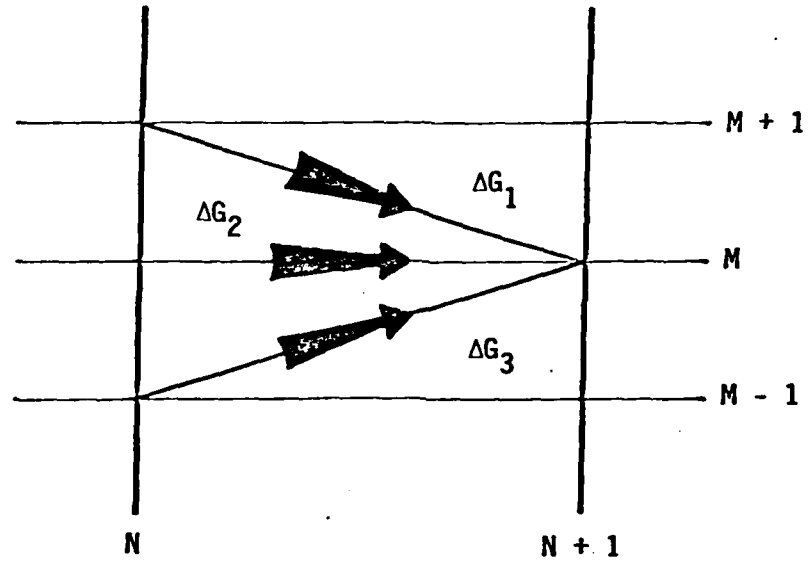


FIGURE 19. Finite-Difference Grid System.

where the kinetics contribution is evaluated as  $G(J,I)_k$  with its associated  $R(J,I)_k$  and  $N(J,I)_k$ . Knowing the category sizes associated with each upstream contribution the Sauter criteria (or other appropriate characterization criteria) can be used to define the new category radius:

$$R(J,I)n+1,m =$$

$$\frac{G(J,I)_k + \Delta G_1 + \Delta G_2 + \Delta G_3}{\frac{G(J,I)_k}{R(J,I)n,m+1} + \frac{\Delta G_1}{R(J,I)n,m} + \frac{\Delta G_2}{R(J,I)n,m-1} + \frac{\Delta G_3}{R(J,I)n,m-1}} \quad (23)$$

Knowing the new mass fraction and size, the number density of particles is determined from:

$$N(J,I)n+1,m = \frac{\rho n+1,m G(J,I)n+1,m}{4/3\pi\rho_L R(J,I)n+1,m} \quad (24)$$

### 3.4 SUMMARY

The particle tracking and boron particle combustion subroutines described in this section represent major developments with respect to the assembly of a modular model formulation for the boron-slurry fueled ramjet combustor. However, considerable further work still remains to complete the modular model development. Some of this work involves the definition of improved models for the kinetics of the boron combustion process and thus requires additional experimental data.

As was noted in the discussion of boron particle combustion models in this section, neither of the models presently available is complete: King's model (Refs. 14, 15) ignores chemical kinetic effects and describes only the ignition stage, while Edelman's model (Refs. 19, 20), which involves kinetically controlled combustion phenomena, ignores the oxide layer in its formulation. Of the two, the most easily extended is the Edelman model, and the generalization of this model to incorporate the effects of the oxide layer on the combustion process is presently being investigated.

Further development with respect to the modeling of two-phase flow phenomena within the context of the modular formulation involves the incorporation within the model of the effects of thermal nonequilibrium and

modeling of the simultaneous oxidation of boron-containing species and the hydrocarbon species in the gas phase. Work in these areas is also in progress.

#### 4. FORMULATION OF A MATHEMATICAL MODEL OF A DUCTED ROCKET COMBUSTOR

The ducted rocket has certain features that are closely related to ramjet systems, particularly integral rocket ramjets which utilize the sudden-expansion ("dump") combustor concept coupled with multiple side entry air inlets. The ducted rocket is sometimes referred to as a gas generator or solid propellant rocket-fueled ramjet. Actually, it is the rocket feature that constitutes the major differentiating feature between ducted rockets and liquid fueled ramjets, since the rocket exhaust, which provides the fuel injection into the ramburner, is choked and its momentum is significant. Because of the underexpansion of the rocket exhaust local supersonic flow is encountered and the significant level of the rocket exhaust momentum relative to the airflow momentum can strongly affect the overall ramburner flowfield. These factors are not present in a liquid fueled ramjet. Significant differences also exist between the ducted rocket fuel, which is made up of the products of combustion of a fuel-rich solid propellant, and the liquid (or slurry) fuels used in ramjets. Further, while practical sudden expansion ramjet combustors can be axisymmetric, ducted rocket configurations, as a rule, are three-dimensional. Thus the analytical simplifications offered by axisymmetry are not available in modeling the ducted rocket flowfield.

Therefore, although there is a logical connection between the combustion processes in ramjets and in ducted rockets, it is clear that there are essential differences that must be addressed in order to establish a better quantitative understanding of the mechanisms and parameters involved in the ducted rocket combustion process. Despite the evident difficulties, development problems that have been encountered clearly show the need for research into ducted rocket combustor aerodynamics: flow patterns, mixing rates, and chemical kinetic rates in ducted rocket environments need to be defined, and analyses tailored to the specific characteristics of the ducted rocket combustion chamber need to be developed.

The complexity inherent in the ducted rocket combustion chamber argues for the use of a modular formulation such as has been successfully developed for axisymmetric liquid fueled sudden expansion ramjet combustor configurations. However, while a data base which provides some description of the combustor

aerodynamics exists for the dump combustor, no such data base exists in the case of the ducted rocket. Since the modular approach depends on an *a priori* description of the size and location of major flowfield elements, particularly regions of recirculating flow, an initial data base is critical to the development of a detailed modular model. In the absence of experimental data, some information on the aerodynamics involved in the ducted rocket combustion chamber flowfield can be obtained through the use of a three-dimensional Navier-Stokes solution procedure. However, this type of modeling is complex and not readily amenable to the incorporation of the detailed chemical kinetics which is also required to gain an overall analytical description of ducted rocket flowfield details. It is, on the other hand, possible to use the Navier-Stokes solution procedure either for nonreacting flow or, using a simple representation of the primary heat release reactions, for reacting flow, to provide the detailed information necessary to construct an appropriate modular model. This is the approach adopted in the present work.

In order to discuss the requirements on a three-dimensional Navier-Stokes solution procedure for the ducted rocket it is useful to consider a specific configuration. To this end, the configuration which is to be utilized in an experimental program at the Aeropropulsion Laboratory (AFWAL) is of interest: a sketch of this configuration is shown in Fig. 20. Basic modeling requirements for the main combustor include the use of the three-dimensional form of the Navier-Stokes equations in cylindrical coordinates, along with a suitable turbulence model and the capability to provide the particle tracking required to compute two-phase flow transport phenomena as outlined in the previous section. For this specific configuration a half-domain computation is sufficient but for generality the capability to compute the full flowfield domain may be necessary.

Two significant complications are inherent with this flowfield. First, the air inlet to the combustor is provided through rectangular ducts, so that the inlet airflow is quite nonuniform, and second, the flowfield in the region of the gas generator nozzles must also be computed. In the latter case, the scale of the flow is significantly smaller than the scale which characterizes the overall flowfield. To adequately handle both of these complications, variable spacing capability is required using both nonuniform mesh spacing and (possibly) coordinate transformations.

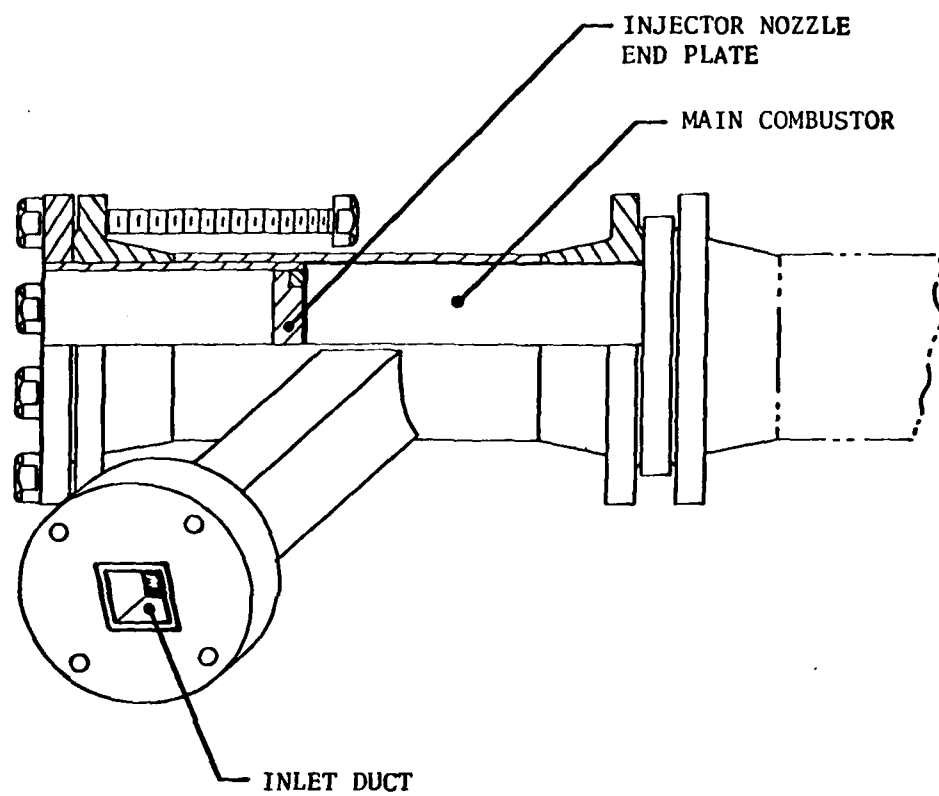


**FIGURE 20. Ducted rocket combustor configuration,  
AFWAL/APL.**

The flowfield within the inlet ducts involves, since recirculations are not expected to be present, a three-dimensional parabolic or quasiparabolic flow. In general, the flow in this duct would be coupled to the conditions within the combustor, but at least as a first approximation an uncoupled analysis can be used. One aspect of this flowfield that requires special attention is the matching of the inlet duct grid with that utilized for the main combustor, as shown schematically in Fig. 21. Matching of grids is also a requirement with respect to the injector nozzle face, as also shown on Fig. 21. The most suitable approach to this aspect of the problem, given the different scales which characterize the injector nozzle and the combustor as a whole is the use of a control volume analysis for the computational region surrounding the injector nozzles.

Development of an aerodynamic model for the combustor shown schematically in Fig. 20 has been based, initially, on the use of the three-dimensional elliptic formulation developed at Imperial College, and described, for example, by Patankar (Ref. 21). This code is a primitive-variables approach, which is to say that it solves the equations for the mean velocity components directly, rather than using transformed variables such as the stream function and vorticity. The solution is obtained iteratively using an underrelaxation technique, with a semi-implicit pressure-correction procedure and a velocity update scheme. For the ducted rocket application the code requires considerable modification, and during this modification effort the structure of the technique is being revised to allow modifications to various aspects of the model (i.e., turbulence models, two-phase flow formulations, and simple chemical kinetics approaches) to be more readily incorporated. The basic code is, however, a steady state formulation; an unsteady-state approach may eventually be required because of the oscillatory nature of the flow that has been observed in some ducted rocket combustor experiments.

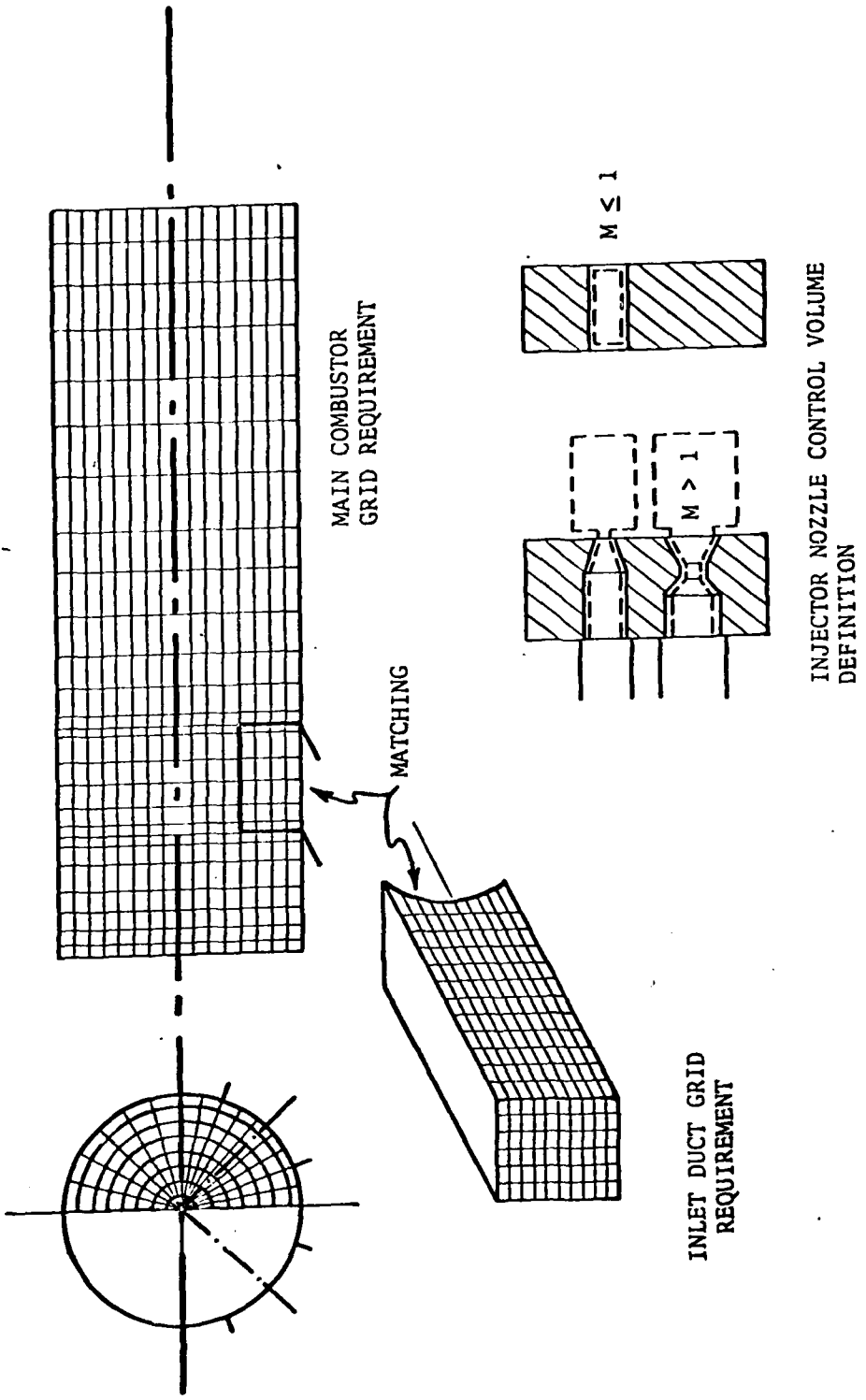


FIGURE 21. Computational grid requirement for ducted rocket combustor computation.

## 5. OVERALL SUMMARY AND FUTURE WORK

Research effort for this period has focused on three major areas of investigation: further examination of the use of the modular ramjet combustor model as a technique for the analysis and interpretation of combustor test data, the development and implementation of a modular model for the boron slurry fueled ramjet, and the development of analytical models for ducted rocket combustors. Further examination of the liquid-fueled ramjet modular model has shown that the stirred-reactor representation of the flame-stabilizing recirculation zones in a dump combustor provides a useful and powerful tool for the examination of dump combustor flame stability characteristics. This work has also demonstrated the utility of the model in terms of the analysis and interpretation of ramjet test data. One area of required future work has been shown to involve the engineering modeling of chemical kinetics phenomena under fuel-rich conditions: in some ramjet designs and under some operating conditions local regions within the combustor, and particularly the recirculation regions, can be considerably more fuel-rich than would be expected based on the overall fuel-air ratio for the operating condition. Engineering chemical kinetics models for fuel-rich conditions are being developed by SAI under other research programs, and future work in this area of the current AFOSR program will involve the incorporation of these models into the modular formulation of the liquid-fueled sudden-expansion ramjet.

Initial work relevant to the boron-slurry fueled ramjet has centered on the analysis and implementation of existing models for boron particle combustion and the development and implementation of a particle tracking technique for use with the modular model formulation. Existing models for boron particle ignition and combustion do not encompass the full range of combustion phenomena relevant to boron combustion necessary to provide a comprehensive model. Future work in this area involves the extension of existing approaches to consider both diffusion- and chemical kinetically-controlled combustion phenomena, including the effects of an oxide surface layer on the particle. The particle tracking methodology developed for use in the modular model provides the only realistic method of computing the combustion behavior of particle clouds, but this approach needs to be extended to include thermal nonequilibrium between the particles and gas phase and the

simultaneous combustion of boron and gas-phase hydrocarbon species. Future work will involve these extensions.

An aerodynamic model for the ducted rocket combustor configuration is under development, based initially on the three-dimensional elliptic formulation developed at Imperial College. Computations of the flowfield within a representative ducted rocket configuration will be carried out during the next year's work. The results of these computations will be used to assess the utility of the approach (including the possibility of there being a requirement for the development of a time-dependent model) and to provide a baseline of flowfield detail required to initiate the development of a detailed modular model of this flowfield.

## 6. REFERENCES

1. Harsha, P. T., and Edelman, R. B., "Mixing and Combustion in High Speed Air Flows," AFOSR TR 80-1005, SAI-80-020-CP, Science Applications, Inc., Canoga Park, CA, July 1980.
2. Edelman, R. B., and Fortune, O., "A Quasiglobal Chemical Kinetic Model for the Finite-Rate Combustion of Hydrocarbon Fuels," AIAA Paper 69-86, 1969.
3. Launder, B. E., Morse, A., Rodi, W., and Spalding, D. B., "Prediction of Free Shear Flows - A Comparison of the Performance of Six Turbulence Models," Free Turbulent Shear Flows, Vol. I, Conference Proceedings, NASA SP-321, 1973, pp. 463-519.
4. Edelman, R. B., Harsha, P. T., and Schmotolocha, S. N., "Modeling Techniques for the Analysis of Ramjet Combustion Processes," AIAA Paper 80-1190, AIAA/SAE/ASME 16th Joint Propulsion Conference, Hartford, Conn., June 30-July 2, 1980. Also AIAA Journal, Vol. 19, No. 5, May 1981, pp. 601-609.
5. Harsha, P. T., and Edelman, R. B., "AFOSR Interim Scientific Report: Mixing and Combustion in High Speed Air Flows," AFOSR-TR-79-0912, SAI-79-013WH, Science Applications, Inc., Canoga Park, CA, April 1979.
6. Harsha, P. T., and Edelman, R. B., "Application of Modular Modeling to Ramjet Performance Prediction," AIAA Paper 78-944, 14th Joint Propulsion Conference, Las Vegas, Nev., July 25-27, 1978.
7. Curran, E. T., "An Investigation of Flame Stability in a Coaxial Dump Combustor," PhD. Thesis, Air Force Institute of Technology, 1979.
8. Schmotolocha, S. N., and Economos, C., "An Experimental Combustion and Flame Stabilization Study of Dump Burners," AFOSR-TR-75-1446, Sept. 1975.
9. Rosfjord, T. J., "Experimental Investigation of Fuel Sprays Formed by Ramburner Injectors," 1979 JANNAF Propulsion Meeting, Vol. 2, CPIA Pub. 300, 1979, pp. 585-607.
10. Pelmas, R. J., et al., "Integral Boost Ramburner Technology for Volume-Limited Missiles," Vol. I, AFAPL-TR-73-55, July 1973.
11. Edelman, R. B., and Harsha, P. T., "Laminar and Turbulent Gas Dynamics in Combustors - Current Status," Progress in Energy and Combustion Science, Vol. 4, No. 1, 1978, pp. 1-62.
12. Hautman, D. J., Dryer, F. L., Schug, K. P., and Glassman, I., "A Multistep Overall Kinetic Mechanism for the Oxidation of Hydrocarbons," Presented at 1980 Technical Meeting, Eastern Section, The Combustion Institute, Nov. 12-14, 1980.

13. "Fundamental Characterization of Alternative Fuel Effects in Continuous Combustion Systems," SAI QPR 029-1, April 15, 1981.
14. King, M. K., "Boron Particle in Hot Gas Streams," Combustion Science and Technology, Vol. 8, 1974, pp. 255-273.
15. King, M. K., "Boron Ignition and Combustion in Air-Augmented Rocket Afterburners," Combustion Science and Technology, Vol. 5, 1972, pp. 155-164.
16. Meese, R. A. and Skifstad, J. G., "Ignition and Global Combustion Models for Clouds of Boron Particles," AIAA Journal, Vol. 12, No. 1 (1974), pp. 71-77.
17. Vovchuk, Y. I. et al., "High Temperature Combustion of an Immobile Boron Particle in an Oxygen-Bearing Medium," Combustion, Explosion and Shock Waves, Vol. 11 (1975), pp. 471-476.
18. Mohan, G. and Williams, F. A., "Ignition and Combustion of Boron in O<sub>2</sub>/Inert Atmospheres," AIAA Journal, Vol. 10, No. 6 (1972), pp. 776-783.
19. Edelman, R. B. et al., "Part III: Theoretical and Experimental Investigation of Metal Particle Combustion in a Supersonic Gas Stream," Gas Generator Fueled Scramjet Program, 1971, AFAPL-TR-70-84, pp. 20-37.
20. Edelman, R. B., Genovese, J., and Fortune, O. F., "Some Aspects of Two-Phase Flows with Mixing and Combustion in Bounded and Unbounded Flows," Journal of Spacecraft and Rockets, Vol. 8, No. 4 (1971), pp. 82-87.
21. Patankar, S. V., "Numerical Prediction of Three-Dimensional Flows," Studies in Convection, Vol. 1, B. E. Launder, ed., Academic Press, New York, 1975, pp. 1-79.